EXTRA CURRENT UNCOVERED

IN

ALKALINE BIOFUEL CELLS

EXTRA CURRENT UNCOVERED
IN
ALKALINE BIOFUEL CELLS

By

CINDY XINXIN ZHAO, B.ENG.

A Thesis

Submitted to the School of Graduate Studies

In Partial Fulfillment of the Requirements

For the Degree

Master of Applied Science

McMaster University

MASTER OF APPLIED SCIENCE (2010) McMaster University

(Materials Science and Engineering) Hamilton, Ontario

TITLE: Extra Current Uncovered in Alkaline Biofuel Cells

AUTHOR: Cindy Xinxin Zhao, B. Eng. (Zhejiang University)

SUPERVISOR: Professor Gu Xu

NUMBER OF PAGES: xi, 74

Abstract

Due to the environmental burden of fossil fuel combustion, a major strategic shift towards renewable green sources and environmentally benign power generation technology makes biofuel cells a possible alternative, though their extremely low current density remains a bottleneck for the further practical applications. Recent progress shows some promise to increase the current by platinum (Pt) electrodes, and alkaline solution to replace the enzymes/microbes. However, the approach involves high cost of noble metals as well as their poisoning effect. We report here a glucose biofuel cell based on nickel (Ni) electrodes and alkaline medium without the catalyst poisoning found in Pt systems. Surprisingly, a six-fold current increase over time, and a final current density equivalent to 1.5 times that of Pt have been achieved. They are found to be caused by the transformation of glucose to an enediol form, the expansion of triple phase boundaries where cathode reactions take place, and the enhancement of reaction kinetics by alkaline solution. The results not only provide a dramatic increase in current and overall biofuel cell performance, but also demonstrate a low cost approach to renewable source utilization, if corresponding designs can be implemented.

Acknowledgements

The author wishes to be deeply grateful to her supervisor, Dr. Gu Xu, for his patient supervision throughout the thesis. The discussion was always helpful and instructive.

The author would like to thank Dr. Yiliang Wu of Xerox Research Center of Canada (XRCC) for UV-Vis measurements and Dr. Quan Yang and Doug K. Charles of Vale Inco Ltd. for their invaluable discussion and great help.

Very special thanks must be given to her group members, Kewei Wang and Han Yan, for their helpful advice and assistance with this thesis.

The author would like to thank her friends, Guozhen Zhu, Feihong Nan and Juan Kong for their friendships and encouragement.

The author wishes to thank her parents, Du Zhao and Hong Chen for providing a positive atmosphere throughout her study overseas. The moral support and confidence of this thesis is greatly appreciated.

The financial support from Ontario Research Fund (ORF), Natural Science and Engineering Research Council of Canada (NSERC), and McMaster University is greatly appreciated.

Table of Contents

List of Figures

List of Schemes

List of Tables

Chapter 1 Introduction

1.1 What is a Biofuel Cell

Biological fuel cells, abbreviated as biofuel cells (BFCs), are electrochemical devices that convert chemical energy directly to electrical energy. Unlike conventional fuel cells, BFCs operate under mild reaction conditions, viz., ambient operation temperature and pressure. It is a genuine fuel cell that holds promise in the long term operation (Shukla, Suresh, Berchmans, Rajemdran, 2004).

It is universally known that fossil fuel combustion causes serious concerns of environmental pollution and resource depletion. The results of the continuous efforts are perceptible, but still modest and very costly. Acid rain remains a serious global threat in spite of the use of sulfur scrubbers. The poor air quality of most of the world's metropolitan areas leads to a severe health threat, though catalytic converters are forced to be installed in all the automobiles to reduce nitrogen oxide and carbon monoxide emissions. More efficient power plants have generated less carbon dioxide per unit of useful energy than did their predecessors, but atmospheric carbon dioxide concentrations continue to rise, intensifying the threat of global warming. Accompanying these diligent efforts to mitigate their environmental burdens, a major strategic shift towards renewable

green sources is bound to achieve more advances and positively impact the potential energy applications.

What the world needs now is a green way to generate electric power efficiently. Among the existing alternatives, hydrogen is the most promising and Proton Exchange Membrane Fuel Cells (PEMFCs) indeed meet the environmental criteria and advance beyond internal combustion engines. Figure 1.1 shows the basic design of a typical PEMFC.

The key components are an anode, to which the fuel is supplied, a cathode, to which the oxidant is supplied, and an electrolyte, which allows the flow of ions (but not the electrons or reactants) between the anode and cathode. The net chemical reaction is exactly the same as if the fuel was burned, but the flow of electrons is produced by spatially separating the reactants. However, PEMFCs are known to be limited by the difficulties associated with hydrogen production and storage, as well as the requirement for platinum (Pt) as the expensive catalyst (Kartha, Grimes, 1994).

To circumvent these problems, the emerging technology of BFCs is rising to directly convert biomass into the electricity from a much wider range of renewable carbohydrates, e.g. glucose, which is nonflammable, nonpoisonous, inexpensive, and easy to handle. Moreover, isolated enzymes or microbes which contain enzymes take the place of Pt to oxidize fuels at the anode (Barton, Gallaway, Atanassov, 2004; Rozenal, Hamelers,

Rabaey, Keller, Buisman, 2008; Logan et al. 2006; Liu, Logan, 2004).

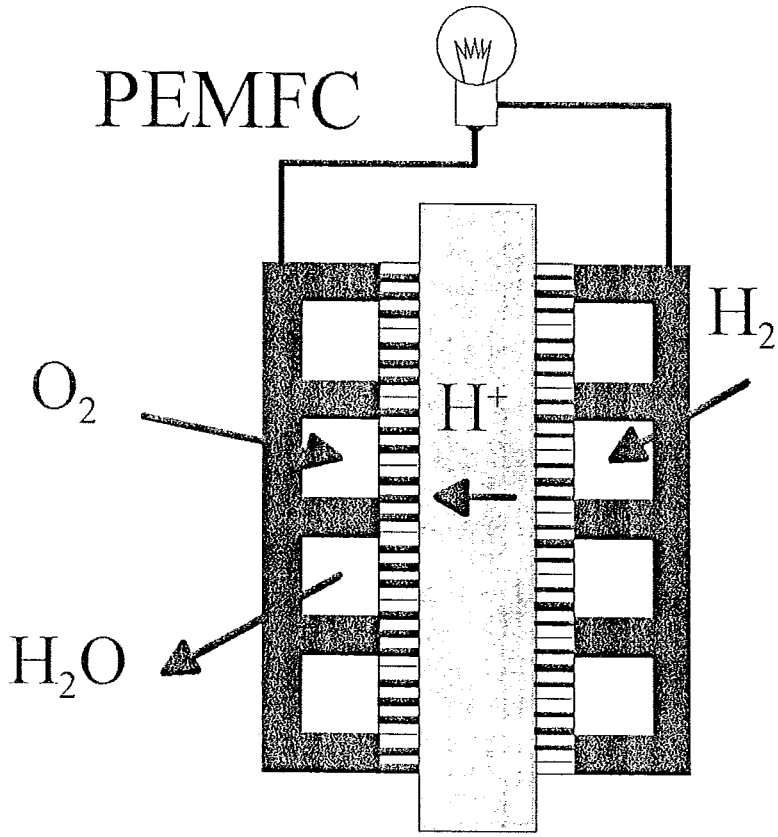

Figure 1.1 A typical PEMFC comsumes reactants and generates a current.

1.2 Working Principle of Biofuel Cells

In general, BFCs employ isolated enzymes or microbes which contain enzymes to catalyze electrochemical reactions to generate electricity, and are operated in room temperature and able to consume liquid form of organic/bio fuels and even wastewater. The working principle of a typical enzymatic BFC is shown in Figure 1.2. At the anode of a glucose consuming BFC, the reduction of glucose with the help of enzymes (E1), such as glucose oxidase (GOx), gives rise to two protons. The bio-catalytic half reaction in the anode side can be summarized as:

$$\text{Anode: } C_6H_{12}O_6 \text{ (glucose)} \rightarrow C_6H_{10}O_6 \text{ (gluconolactone)} + 2H^+ + 2e^- \qquad (1.1)$$

The electrons produced in the anodic reaction are transferred to the electrode and protons flow through a proton exchange membrane (PEM) to the cathode. In order to increase the electron transfer efficiency, an electron transfer mediator (M1) is necessary in the anode chamber. At the cathode, oxygen molecules dissociate into atoms, which combine with the electrons and the migrating protons to form water. The cathodic reaction is catalyzed by another kind of enzyme (E2), such as laccase. Similarly, another electron transfer mediator (M2) is needed in the cathode side. The half reaction at the cathode can be summarized as:

Cathode: $1/2\ O_2 + 2H^+ + 2e^- \rightarrow H_2O$ (1.2)

The whole cell reaction is thus:

Overall: $C_6H_{12}O_6$ (glucose) $+1/2\ O_2 \rightarrow C_6H_{10}O_6$ (gluconolactone) $+ H_2O$ (1.3)

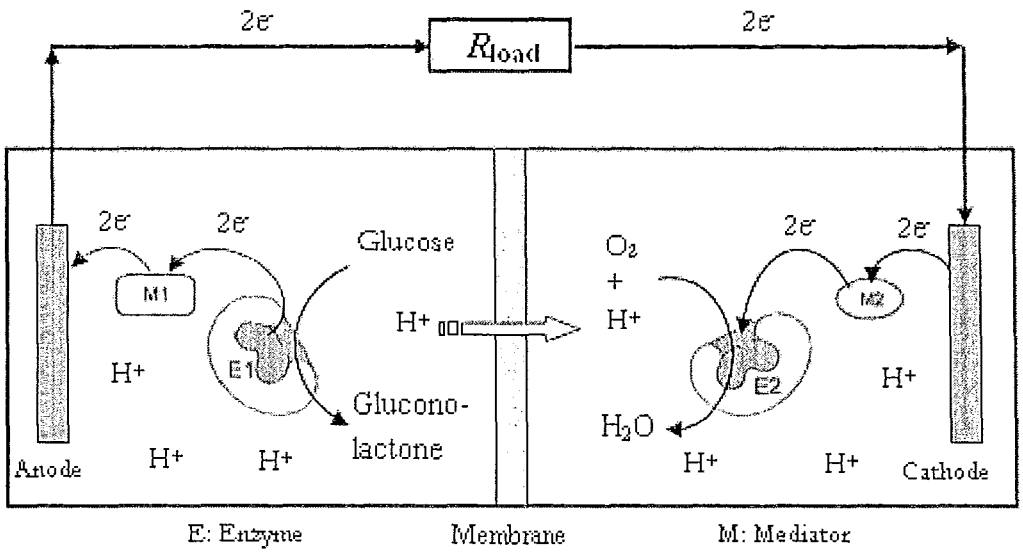

Figure 1.2 The working principle of an enzymatic BFC (Zhi, 2006)

As described in Figure 1.2, both reactions occur in the solution. Therefore electrons produced in the anode compartment must pass through enzyme E1 to mediator M1, then to the electrode, and then through an external circuit to the cathode. The electron transfer in the cathode compartment cannot be achieved without mediator M2 and enzyme E2.

Basically, microbial BFCs operate in the same way as enzymatic BFCs. The only difference is that microbes are utilized as biocatalysts in microbial BFCs. By involving the complete multi-enzyme metabolic pathways inside living cells, microbial BFCs exhibit unique features unmatched by enzymatic BFCs, such as long-term stability and complex fuels utilization. Nevertheless, the power densities of microbial BFCs are typically much lower owing to the resistance caused by mass transfer across the cell membranes of microbes. On the other hand, enzymatic BFCs demonstrate reduced stability because of the selectivity and limited lifetime of extracellular enzymes. However, higher power densities can be obtained by specific designs of enzymatic BFCs possessing the enzyme-immobilized or enzyme-entrapped electrodes, especially when the enzymes are used in the concentrated form (Barton, Gallaway, Atanassov, 2004).

1.3 Future Applications of Biofuel Cells

BFCs were once put into the market in the 1960s and gradually lost the market share in the competition with other energy devices, such as solar cells. After decades of research, they have been the center of attention again (Zhi, 2006).

BFCs copy nature's solutions to energy generation. They consume renewable biomass from the nature. The energy released during the complete route of glucose

oxidizing to CO_2 and water is about 16×10^6 J/kg, equivalent to 5 kWh of electrical energy. Therefore a medium-sized car with energy transformation of 200 Wh/km could travel 25 to 30 km on 1 kg of a concentrated sugar solution in theory (Shukla, Suresh, Berchmans, Rajemdran, 2004).

Implantable devices or sensors can be achieved according to the working principle of BFCs. These medical devices can utilize glucose, a sugar present in the blood system, as fuel, and can generate power as long as the subject lives (Figure 1.3A). One more interesting application is a BFC powered robot (Figure 1.3B). The "Gastrobot" is thought to be the first robot of its kind to use such a novel biomass energy conversion method (Wilkinson, 2000).

Referring to electronics, BFCs have demonstrated their potential. SONY in 2007 announced the development of an enzymatic "sugar-cell" using glucose and various mediators in a system with membrane (SONY, 2007). The total output power was 50mW (1.5 mW/cm2), which was enough to run a portable mp3 player during the demonstration for a few seconds. However, SONY didn't mention the durability of the inv ention, another feature in order to make it commercialized. In 2010, a Chinese designer Daizi Zheng has created a conceptual mobile phone for Finnish brand Nokia that could be powered by sugary drinks as shown in Figure 1.3C (Anita, 2010). Zheng proposes that the phone could run on a biobattery that uses enzymes to generate electricity from

carbohydrates.

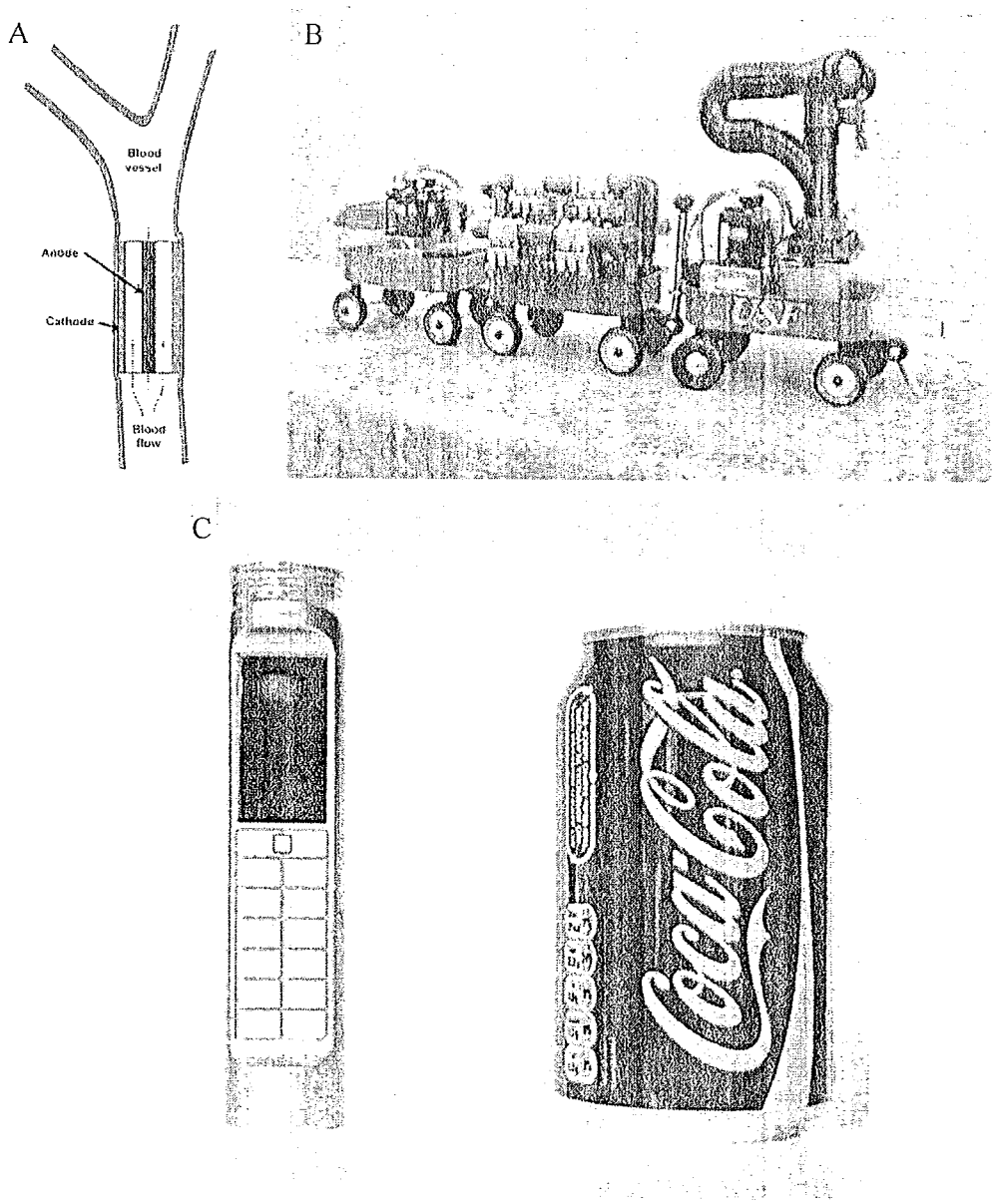

Figure 1.3 Applications of BFCs. (A) a BFC directly attached to the blood vessel (Haselkorn, 2002), (B) "Gastrobot" (Wilkinson, 2000), (C) a conceptual mobile phone for Finnish brand Nokia that could be powered by sugary drinks (Anita, 2010)

1.4 Problem Statement

Due to the environmental burden of fossil fuel combustion, a major strategic shift towards renewable green sources and environmentally benign power generation technology makes biofuel cells a possible alternative, though their extremely low current density remains a bottleneck for the further practical applications. The performance of BFCs, in terms of power density, is three to four orders of magnitude lower than a typical PEMFC of about 1 W/cm^2. In fact, many applications for BFCs require a power output in the range of 10~100 mW/cm^2.

Recent progress shows some promise to increase the current by Pt electrodes, and alkaline solution to replace the enzymes/microbes. However, the approach involves high cost of noble metals as well as their poisoning effect. Thus, a non-Pt metal has to be considered, involving electrocatalytic activity towards the oxidation of glucose. Among the choices, Ni is chosen for its well established catalytic mechanism and success in other bio related devices. It is, therefore, the purpose of this thesis to study a glucose BFC, based on Ni foams and alkaline medium. Moreover, a six-fold current increase over time, and a final current density equivalent to 1.5 times that of Pt have been achieved in the experiments. Therefore, this thesis will discuss the origin of the "extra" current and the related phenomenon.

1.5 Thesis Overview

The thesis consists of seven chapters. Chapter 1 provides the introduction of BFCs, including the definition, motivation, working principle and potential applications. Chapter 2 involves literature review, including the main problems of BFCs and possible solutions. Chapter 3 details the experimental methods and instruments. Chapter 4 provides the initial exploration of resolving pH gradient problem. Chapter 5 uncovers the "extra" current found in alkaline biofuel cells. Chapter 6 presents the conclusions and Chapter 7 the future work.

Chapter 2 Literature Review

2.1 Problems of Biofuel Cells

In spite of the advantages of BFCs described in the previous chapter, conventional glucose BFCs are still not commercially available, which are mainly limited by a few important factors to be described as follows.

2.1.1 Low Power Density and Current Density

The performance of BFCs, in terms of power density, falls far below that of PEMFCs. Conventional enzymatic BFCs have the power output of 0.05 mW/cm^2 to 0.3 mW/cm^2 (Katz, Willner, 2003; Soukharev, Mano, Heller, 2004; Tsujimura, Kano, Ikeda, 2002). The best reported power density so far has been 1.45 mW/cm^2, using a glucose dehydrogenase-entrapped carbon-fiber anode and a bilirubin oxidase (BOD)-immobilized cathode, which is still three orders of magnitude lower than a typical PEMFC of about 1 W/cm^2 (Sakai et al. 2009). There is a credibility gap that must be bridged if BFCs are to find a practical application (Figure 2.1). In fact, many applications for BFCs require a

power output in the range of 10～100 mW/cm^2.

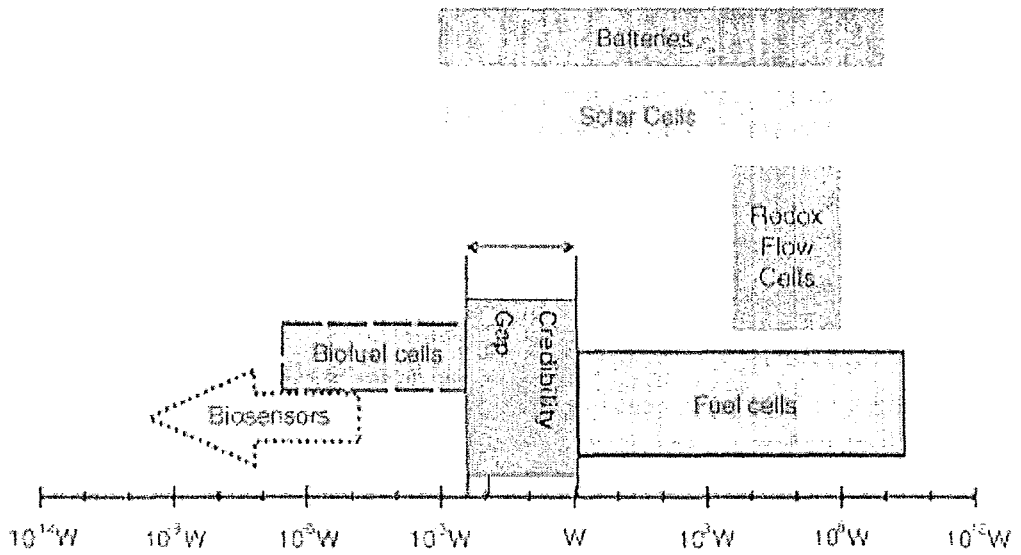

Figure 2.1 Approximate power output ranges of biosensors, biofuel cells and inorganic fuel cells, illustrating the scale of the credibility gap challenging the biofuel cell researchers (Bullen, Arnot, Lakeman, Walsh, 2006).

Due to the similarity of the output voltages, which are based on the redox potentials, the low current density restricts the BFC operation and becomes the primary challenge.

2.1.2 pH Gradient Problem and Possible Solutions

Found in 2006, a pH gradient problem jeopardizes further applications of BFCs (Rozendal, Hamelers, Rabaey, Keller, Buisman, 2008; Rozendal, Hamelers, Buisman, 2006; Zhi, 2006; Rozendal, Hamelers, Molenkamp, Buisman, 2007). It is associated with proton transport in Nafion.

A dramatic decrease of pH in the anode limits the power density of the system, due to the nature of membranes which are conducting ion species other than protons to maintain electroneutrality, thus the protons are accumulated in the anode rather than penetrating into the cathode. Simultaneously a slowdown of electron transfer via the external circuit takes place. In addition, the concentrations of other cations in the anolyte are significantly higher than that of protons, making proton transport negligible. Analysis of the Nafion membrane taken from the set-up of Rozendal et al (2006) shows that K^+ and Na^+ take up 74% of the sulfonate residue.

Furthermore, Chae et al (2008) confirmed this result using X-ray (EDX) analysis. The relative atomic percentages of carbon and fluoride are lowered in a piece of used Nafion, compared with the new one. At the same time, sodium and iron which should not exist in Nafion, increase in percentage and those atoms hinder the proton transport.

When going back to the fundamentals, it becomes evident that the pH gradient problem is manifested by the buffer solution, the pH value and the membrane electrolyte.

The pH value of the anolyte is fixed by the living conditions of enzymes in our case, therefore no change can be made. However, the types of membranes, viz., CEM or anion exchange membrane (AEM) are variable or controllable.

AEM BFCs were introduced in 2007 based on the electrohydrogenesis system (Rozendal, Hamelers, Molenkamp, Buisman, 2007). They concluded that in terms of the ability to prevent large pH gradient at the anode and cathode, AEM were better off. However, AEM caused higher overpotentials at the cathode. Kim et al (2007) have done similar work and their first paper involved direct comparison of different membranes in a microbial BFC system. AEM showed the highest power output among all the candidate membranes including Nafion.

2.1.3 Complex Nature of Biocatalyst

It is universally known that the kinetics of the bio-reactions is intrinsically slow due to the complex nature of biocatalysts. The electrons transfer from the oxidation sites inside the enzymes finally to the electrodes (Barton, Gallaway, Atanassov, 2004; Bullen, Aront, Lakeman, Walsh, 2006). Enzymes have a complex structure comprised of proteins. The electron transfer unit of enzymes, viz., the active center, is surrounded by its protein matrices. Hence, efficient electrical communication between electrode and enzymes is

difficult.

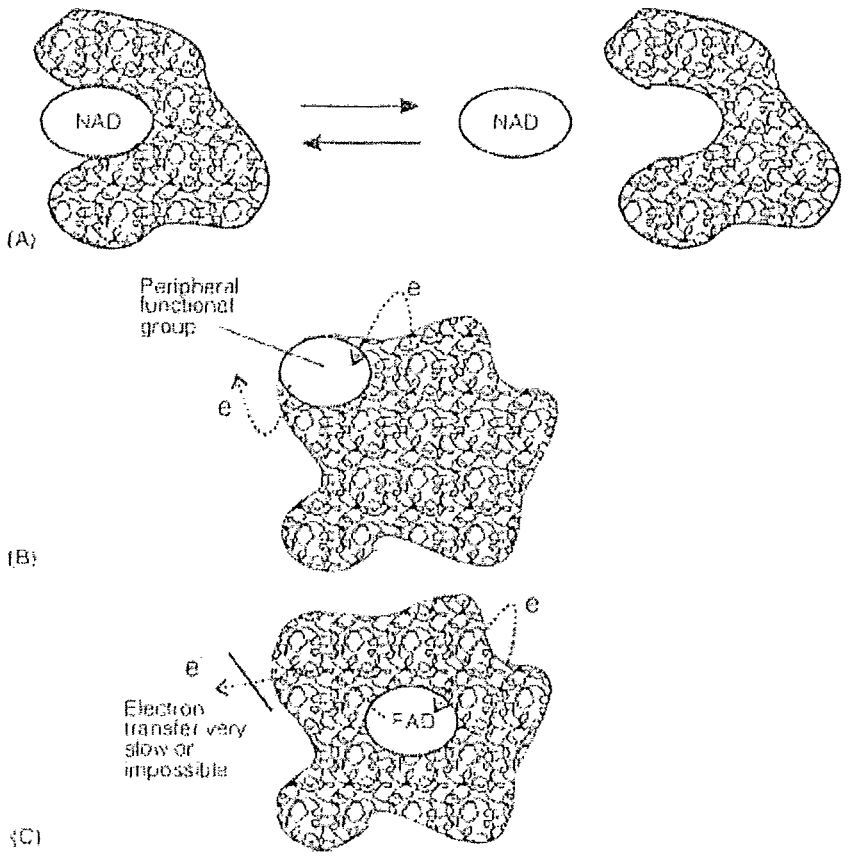

Figure 2.2 The different locations of enzyme active centers and how they affect electron transfer in unmodified enzymes. (A) Enzyme active center is NAD(H) or NADP(H). (B) The active center is located on the periphery of the enzyme. (C) The enzyme has strongly bound redox centers, surrounded by the glycoprotein shell (Bullen, Aront, Lakeman, Walsh, 2006).

Enzymes can be divided into three groups when discussing methods of establishing electron transfer between enzymes and electrode (Figure 2.2).

The first group has enzymes with Nicotinamide Adenine Dinucleotide (NADH/NAD+) or Nicotinamide Adenine Dinucleotide Phosphate (NADPH/NADP+) redox centers (e.g. lactate dehydrogenase), which are often weakly bound to the protein of the enzyme. The active center can diffuse out of the enzyme and travel to the electrode, transferring electrons itself.

In the second group of enzymes at least part of the redox center is conveniently located at or near the periphery of the protein shell (e.g. peroxidases). The active center (often porphyrin derivatives) is located on the periphery of the enzyme, and can transfer electrons directly to (or receive electrons from) the electrode.

The third type of enzymes has a strongly bound redox center (e.g. Flavin Adenine Dinucleotide (FAD)), which is deeply bound in a protein or glycoprotein shell. Direct electron transfer from the active center is either extremely slow or impossible, requiring the use of mediator molecules capable of penetrating into the enzyme to transport charge. In this case, GOx is the most studied for BFCs.

In general, electron transfer between the enzyme and electrode is classified by two different mechanisms (Figure 2.3): direct electron transfer (DET) and mediated electron transfer (MET). Depending on the enzymes and reaction conditions, rates of MET can

exceed by orders of magnitude those of DET (Barton, Gallaway, Atanassov, 2004)

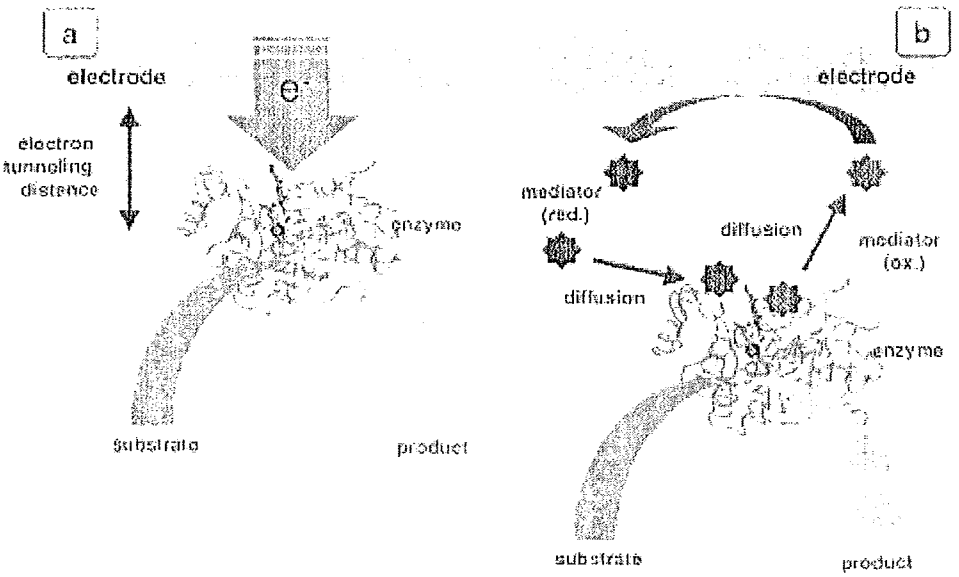

Figure 2.3 (a) Direct electron transfer from the electrode surface to the active site of an enzyme, (b) Electron transfer via the redox mediator (Barton, Gallaway, Atanassov, 2004)

Although the mechanisms of electron transfer have been established, the effective transfer is still limited by the complex nature of biocatalysts and relevant bioreactions, and hence several activation energies are encountered as shown in Figure 2.4, which decrease the BFC performance dramatically.

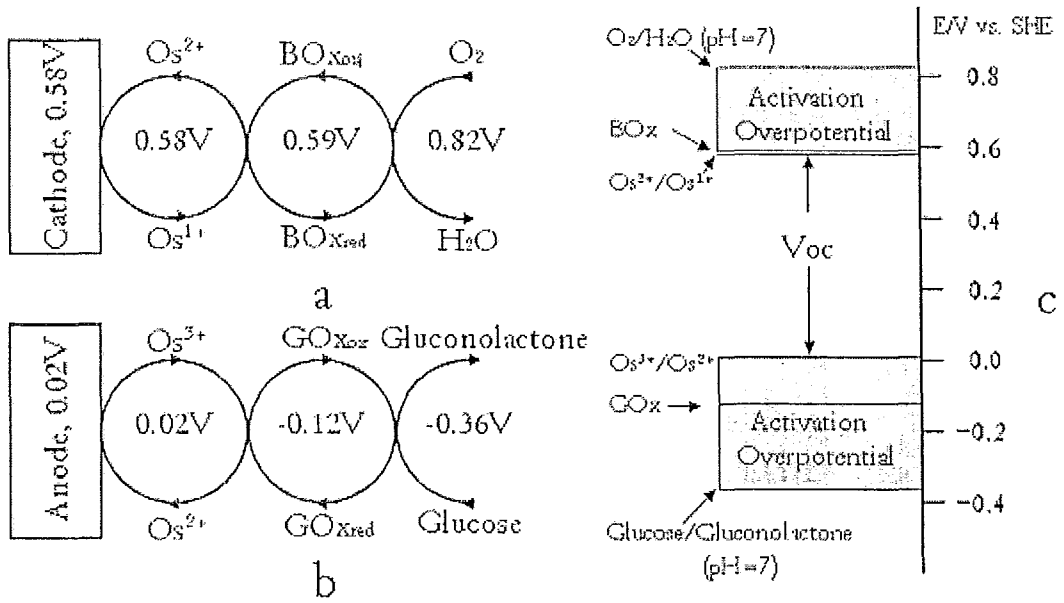

Figure 2.4 Several activation energies are encountered, leading to an output voltage loss as the activation overpotential (Barton, Gallaway, Atanassov, 2004)

2.2 Attempt by Others to Increase Output

Recently, a solution to all these problems has been proposed by Fujiwara et al, who introduced a new type of glucose BFC, which for the first time employed noble metal and alkaline media to replace enzymes or microbes (2009). The maximum power density and nominal short-circuit current density were reported to be 20 mW/cm^2 and 85

mA/cm^2, which are 80-100 times higher than that of conventional enzymatic BFCs.

2.2.1 Biofuel Cell Operation

This non-enzymatic BFC operates as shown in Figure 2.5. At the anode, the oxidation of glucose assisted by hydroxyls on Pt catalyst produces water and electrons which pass through the external load. At the cathode, oxygen molecules dissociate, and then combine with the electrons and water to form hydroxyls, which migrate through the anion exchange membrane toward the anode.

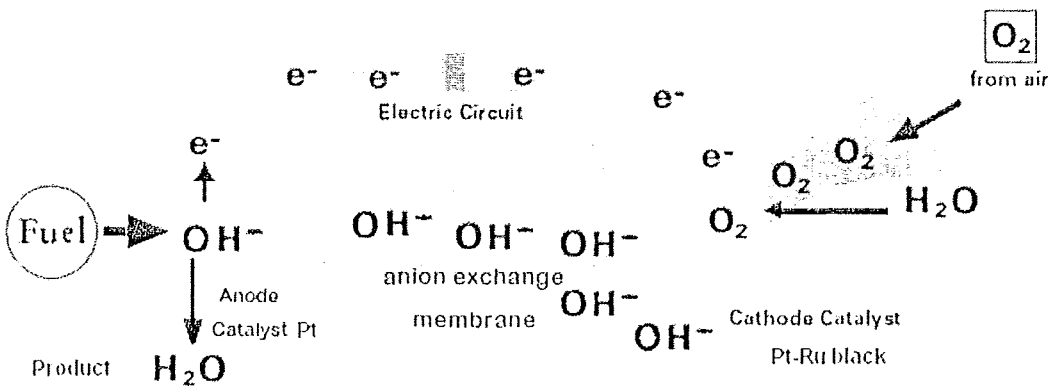

Figure 2.5 The working principle of the non-enzymatic BFC

Therefore, the anodic reaction becomes a two-electron oxidation of glucose to gluconic acid and the cathodic reaction oxygen reduction reaction. The overall reaction of the BFC is equivalent to the combination of the above two half-cell reactions.

Anode: $C_6H_{12}O_6$ (glucose) + 2 OH^- → $C_6H_{12}O_7$ (gluconic acid)+ H_2O +2e^- (2.1)

Cathode: 1/2 O_2 + H_2O +2e^- →2 OH^- (2.2)

Overall: $C_6H_{12}O_6$ (glucose) +1/2 O_2 → $C_6H_{12}O_7$ (gluconic acid) (2.3)

The theoretical voltage calculated under standard conditions is 1.256 V, based on the redox potentials of -0.853 V and 0.403 V for the anodic and cathodic reactions, respectively. This is very similar to that of PEMFCs of 1.23 V.

2.2.2 New Problems Arise

However, the high cost of Pt still remains in the above system. The glucose oxidation process at the anode generates two electrons, and leaves behind an adsorbed intermediate, gluconolactone (finally hydrolyzed to gluconic acid), which acts as a poison for the catalyst and prevents further oxidation of additional glucose in the compartment.

This poisoning effect is manifested in the polarization curve. A retrograde polarization curve appeared, when the above results were duplicated, which was found to be due to the Pt poisoning effect. Experimentally, the current first increases then decreases accompanied by the drop of the load resistance and the output voltage. This can be explained by the increasing poisoning rate at higher current densities overwhelming the anodic oxidation rate (Sandia Report, 2005).

2.3 Other Electrocatalytic Metals Applied in Biofuel Cells

Because of this poisoning effect of Pt catalyst, a non-Pt metal has to be considered, which involves certain electrocatalytic activity towards the oxidation of glucose. Among the choices, nickel (Ni) is widely studied. For example, Fleischmann first studied Ni electrodes and explained the oxidation of alcohols and amines on the basis of a mechanism involving electron-transfer mediation by a $Ni(OH)_2$/NiOOH redox couple at the anodized electrode surface (Fleischmann, Korinek, Pletcher, 1971; Fleischmann, Korinek, Pletcher, 1972). A similar mechanism has been proposed by Luo et al to explain the anodic oxidation of glucose on Ni electrodes in alkaline medium (Luo, Zhang, Baldwin, 1991). Furthermore, enzymeless glucose detection has been performed at a metallic Ni electrode and other Ni based electrodes (Zhao, Shao, Li, Jiao, 2007).

The feasibility of Ni in oxidizing glucose suggests, a glucose BFC based on Ni in alkaline medium might become a valid solution. It is, therefore, the purpose of this thesis to study a glucose BFC, based on Ni foams and alkaline medium.

Chapter 3 Experimental Details

3.1 Biofuel Cell Design and Construction

3.1.1 Biofuel Cell Design

A schematic of BFC design is shown in Figure 3.1. Our biofuel cell is composed of a metal-based anode and cathode. The anode and cathode compartments are separated by a membrane which allows the flow of specific ions but not water or electrons. The anode and cathode compartments (working volume of 45ml each) were made from plexiglass tubes. Each side of plexiglass tubes was fitted with two ports. These ports serve as gas and electrolyte inlets and outlets. There are two O-rings on plexiglass covers and four O-rings on Teflon plates to provide an electrolyte tight seal. Two 3.9375"×3.937"× 0.5" Teflon plates and two stainless steel covers are to tighten the plexiglass tubes by six fastening parts consisting of bolts, washers and nuts. Thus, a good electrolyte tight seal and a good electrical contact are attained.

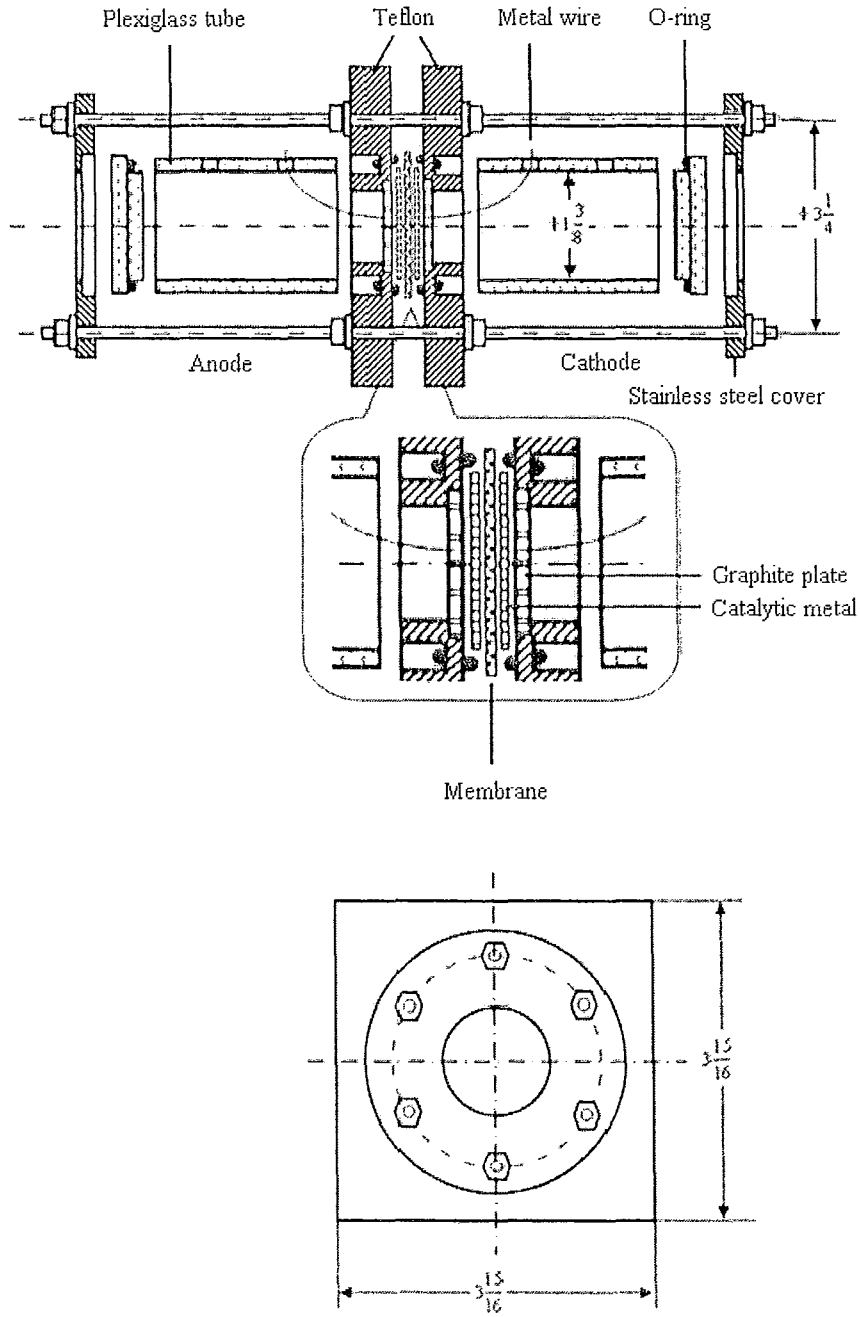

Figure 3.1 Schematic diagram of the BFC

3.1.2 Enzymatic Biofuel Cell Construction

Carbon paper (E-TEK Inc.) and carbon paper with 2.0 mg/cm^2 Pt loading (30% Pt-C black, single sided V2 ELAT, E-TEK Inc.) were used as the electrodes at the anode and cathode, respectively, by which ion exchange membrane was directly sandwiched, without applying any powder or paste. To ensure the intimate contact between the carbon papers and membrane, two graphite plates (Speer Canada Inc.) with 21× Φ 2 mm holes were used as current collectors and backing plates outside the carbon paper-membrane sandwich. The nominal surface area of the electrodes measures 0.66 cm^2. The sandwich structure as well as the graphite plates were mounted in between two chambers to form a enzymatic BFC. Pt wire connecting these graphite plates passes through the ports at the plexiglass tubes to be connected to the external circuit.

3.1.3 Nickel-based Biofuel Cell Construction

Ni foams (250 μm pore size and 90% porosity, Vale Inco Ltd.) were used as catalytic electrodes at both the anode and cathode, by which an anion exchange membrane (ion exchange capacity: >1.2meq/g, Fumasep™ FAB) was directly sandwiched, without applying any powder or paste. The nominal surface area of the

electrodes measures 2.30 cm^2. To ensure the intimate contact between the Ni and membrane, two graphite plates were used as backing plates outside the Ni-membrane sandwich. The sandwich structure as well as the graphite plates were mounted in between two chambers to form a Ni-based BFC. Ni wire connecting Ni foams passes through the ports at the plexiglass tubes to be connected to the external circuit.

3.1.4 Platinum-based Biofuel Cell Construction

Two carbon papers with 2.0 mg/cm^2 Pt loading (30% Pt-C black, single sided V2 ELAT, E-TEK Inc.) were used to duplicate Fujiwara's results. They were hot pressed together with the anion exchange membrane to form the membrane electrode assembly (MEA), as described in the literature (Ren, Wilson, Gottesfeld, 1996). Similarly, the MEA was supported by graphite plates, functioning as current collectors, and mounted in the cell. Pt wire connecting these graphite plates passes through the ports at the plexiglass tubes to be connected to the external circuit.

3.2 Membrane, Anolyte and Electrode Preparation

3.2.1 Membrane Pretreatment

Nafion 117 purchased from DuPont, was pretreated with a standard cleaning procedure: (i) boiling in 3% hydrogen peroxide for 1 hour to oxidize organic impurities; (ii) rinsing in boiling water for several hours; (iii) boiling in 1M sulfuric acid for 1 hour to remove any metallic/ionic impurities; and (iv) rinsing again in boiling water to remove any excess acid.

AMI-7001 (AEM) was purchased from Membranes International Inc., USA.

Fumasep™ FAB (AEM) was purchased from FuMa-Tech, Germany.

EXCELLION I-100 (AEM) was purchased from Snowpure, USA.

Anion Exchange Membranes were prepared in unsealed containers in 3 wt% KCl solution. To control and minimise wrinkling, it is recommended to expand membranes before cutting and stack assembly by equilibration in KCl solution for at least 24 hours.

After pretreatment, membranes were stored in the same solution to keep from drying out since micro cracks may likely occur during shrinkage.

3.2.2 Anolyte Preparation

Glucose Oxidase (GOx) was purchased from Sigma-Aldrich, Canada, with the enzyme activity of 216 U/mg. (1U corresponds to the amount of enzymes used to oxidize

1μ mol glucose per minute at pH = 7.0 and 25℃).

Phosphate buffer solution (0.1 M, measured pH 7.23) was made from Na_2HPO_4 and NaH_2PO_4 (Sigma-Aldrich, Canada).

Tris buffer solution (0.1 M, measured pH 7.20) was made from Tris buffer (Sigma-Aldrich, Canada).

Glucose (Sigma-Aldrich, Canada) in the phosphate buffer was allowed to mutarotate for 24 hours before use.

Ferrocene Monocarboxylic Acid (FMCA) was purchased from Sigma-Aldrich, Canada.

Glucose alkaline solution (0.5 M) was made from 0.5 M D-glucose and 0.5 M KOH, which were purchased from Sigma-Aldrich, Canada.

Glucose neutral solution (0.5 M) was made from 0.5 M D-glucose and 0.5 M KCl, which were purchased from Sigma-Aldrich, Canada.

All solutions were prepared with deionized water.

3.2.3 Electrode Preparation

Ni foams were pretreated with a clean procedure by: (i) rinsing in 3% hydrogen peroxide for 1 hour to oxidize organic impurities; (ii) rinsing in boiling water for several

hours; (iii) rinsing in 0.5M KOH for 1 hour to remove any metallic/ionic impurities; and (iv) rinsing again in boiling water to remove any excess alkali. The foams were dried in the vacuum oven at 60 ℃ for 10 mins and then set aside when cooling down.

The graphite plates were cleaned with 0.5 M HCl followed by 0.5 M KOH after each experiment and stored in distilled water before use.

3.3 Experimental Set-up

Figure 3.2 shows the experimental set-up for the BFC operation and measurement apparatus. The performance of the BFC was evaluated at room temperature and atmospheric pressure by supplying N_2 gas to the anode compartment to keep anoxic, and humidified oxygen to the cathode compartment. The gassing rate to each compartment was 10 ml/min. The variable loading for the testing cell was controlled by a variable resistor. Multimeters were used to measure the cell current, voltage and potential difference between electrodes and the reference electrode. Experimental data acquisition in a personal computer was controlled by general purpose interface bus (GPIB) interface, along with programs written in Quick Basic as experiment progressed.

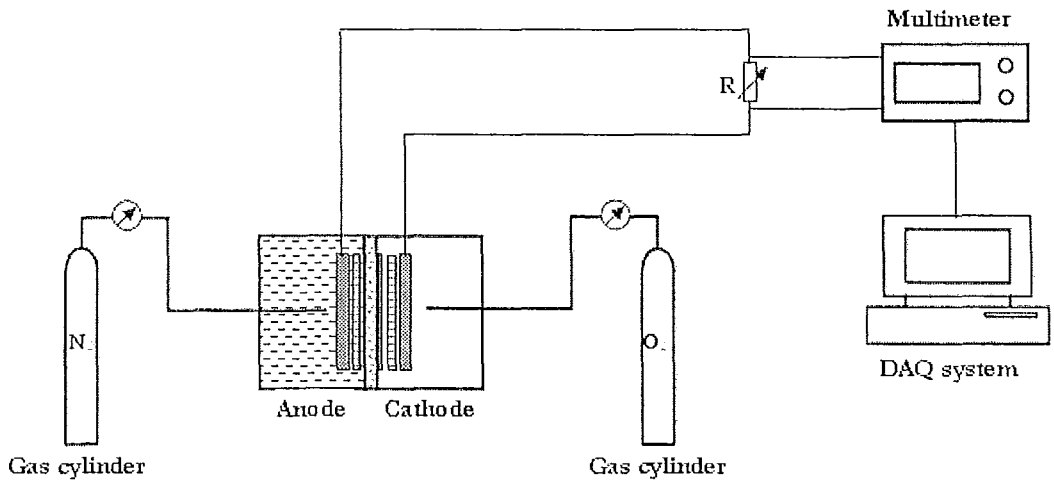

Figure 3.2 Schematic of BFC operation and measurement apparatus

3.4 Polarization Curve Measurement

Polarization curve refers to the relationship between the output voltage and current under variable resistance loading. Cell current and output voltage were monitored and measured by HP 3478A digital multimeter (Electrolab Inc., USA) from open-circuit to short-circuit. The BFC was allowed to equilibrate at open circuit for about 0.5 to 1 hour, until the open circuit potential was stabilized. The loading between the electrodes was lowered step by step, pausing at each resistance setting for 5 minutes. The cell current and

voltage were measured and recorded by the same time intervals, assuming a steady state was reached. Generally, it takes about 90 minutes to make one IV curve measurement. The power extracted from the BFC was obtained by $V_{cell} \times I_{cell}$, and it can also be estimated by $(V_{open\text{-}circuit} \times I_{short\text{-}circuit})/4$. The current and power densities were then obtained by the cell current and power divided by the effective surface area.

3.5 pH Measurement

The pH values were measured by ExStik pH 110 meter (Extech Instrument Corporation, USA) which was calibrated carefully before the measurements.

3.6 Ultraviolet-visible Spectroscopy Measurement

Ultraviolet-visible spectroscopy (UV-Vis) refers to absorption spectroscopy in the UV-visible spectral region. It uses light in the visible and adjacent (near-UV and near-infrared (NIR)) ranges. The absorption in the visible range directly affects the perceived color of the chemicals involved. In this region of the electromagnetic spectrum, molecules undergo electronic transitions from the ground state to the excited state.

The wavelengths of absorption peaks can be correlated with the types of bonds in

a given molecule and are valuable in determining the functional groups within a molecule. The spectrum alone is not, however, a specific test for any given sample. The nature of the solvent, the pH of the solution, temperature, high electrolyte concentrations, and the presence of interfering substances can influence the absorption spectrum. When UV/vis spectroscopy is applied to the analysis, these variables must be controlled or accounted for in order to identify the substances present.

Chapter 4 Exploring the pH Gradient Problem

4.1 pH Gradient Problem Confirmed

Since 2006, it has been realized that the transportation of protons in Nafion, cation exchange membranes (CEM), is hindered by the low concentration of protons in the neutral anolyte compared with other cations, e.g., Na^+, which are introduced by the buffer solution. Because of the neutral environment required by enzymes or microbes, pH value of about 7 leads to the ratio of other cations over protons to be about 10^6 to 10^7. Owing to the nature of Nafion, a large portion of Na^+ cations are transported by the membrane to maintain the closed electron/ion circuit and thus protons are accumulated in the anode, rather than penetrating into the cathode. Therefore a dramatic decrease of pH in the anode is observed, as well as a simultaneous slowdown of electron transfer. In addition, the pH gradient problem has an immediate effect on the low power density output.

Our enzymatic BFC was operated on the basis of

$$\text{Anode: } C_6H_{12}O_6 \text{ (glucose)} \rightarrow C_6H_{10}O_6 \text{ (gluconolactone)} + 2H^+ + 2e^- \quad (4.1)$$

$$\text{Cathode: } 1/2\ O_2 + 2H^+ + 2e^- \rightarrow H_2O \quad (4.2)$$

Overall: $C_6H_{12}O_6$ (glucose) +1/2 $O_2 \rightarrow C_6H_{10}O_6$ (gluconolactone) + H_2O (4.3)

According to the results of Zhi (2006), the optimized concentrations of glucose, GOx and FMCA in our enzymatic BFCs are 200 mmol/L, 0.6 g (based on 50 mL) and 4 mmol/L, respectively. Although the set-up of Rozendal et al (2006) is based on a microbial BFC, a similar phenomenon in our enzymatic BFC was observed. The pH value decreased from 6.74 to 6.08 after 7 day operation as depicted in Figure 4.1, where the first data point was measured right after the enzyme was added.

4.2 Fundamental Analysis

When going back to the fundamentals, it becomes evident that the pH gradient problem is manifested by the buffer solution, the pH value and the membrane electrolyte. The pH value of the anolyte is fixed by the living conditions of enzymes in our case, therefore no change can be made. However, the type of membranes, viz., CEM or anion exchange membrane (AEM), and the specific cations in the buffer solution are variable or controllable.

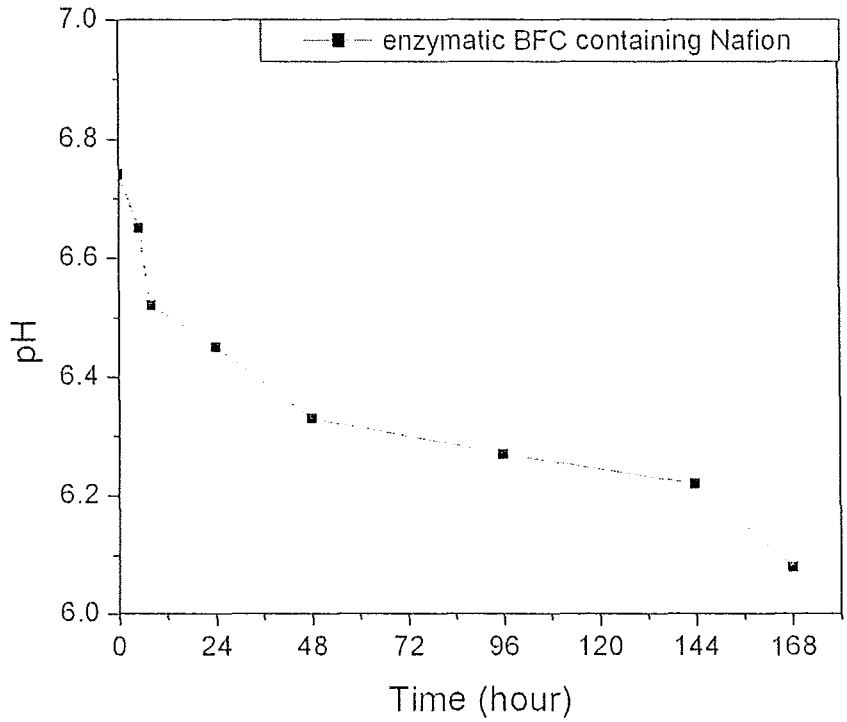

Figure 4.1 The pH value decreased from 6.74 to 6.08 after 7 day operation in our enzymatic BFC containing Nafion.

4.3 Tris Buffer

Tris/TrisH$^+$ buffer was first tested under the physiological condition. In our proposed mechanism in Tris buffer based enzymatic BFC, the cation, viz., NH^{3+} , has little or no negative effect on proton transport in Nafion, because of the bigger ionic size

than that of Na^+ and the ion selectivity of the membrane. At the anode, proton accumulation caused by oxidation reactions tends to decrease the pH value. However, a $CNH_2(OH)_3$ group can absorb a proton to form $CNH_3(OH)_3^+$, resulting in the mitigation of the tendency to increase the acidity.

Experimentally, a Tris buffer with the same ionic strength as phosphate buffer was used to dissolve glucose and mediators. Stirred ultrasonically at room temperature for a sufficiently long time, the solution was found with residual undissolved FMCA, in spite of the fact that the same amount could easily be dissolved in the phosphate buffer solution at the same temperature.

The performance test of this Tris buffer based BFC was conducted using Nafion as the membrane. A figure of pH vs. time (figure 4.2) was plotted while an external load was connected to our BFC. The first data point was measured right after the enzyme was added.

Obviously, the expected pH stabilization has not been achieved. Compared with the pH drop vs. time in our Nafion based BFC (figure 4.1), it produces a more severe pH decay. The experiment of Tris buffer based BFC was halted within 24 hours, because it showed no sign of leveling the pH gradient across the membrane.

Therefore, Tris/$TrisH^+$ buffer is not an ideal alternative that can potentially solve the problem of pH gradient across the membrane. Nevertheless, it still remains a

challenge to further search other organic buffer solutions. It is therefore inconclusive, before exhausting other appropriate organic buffers.

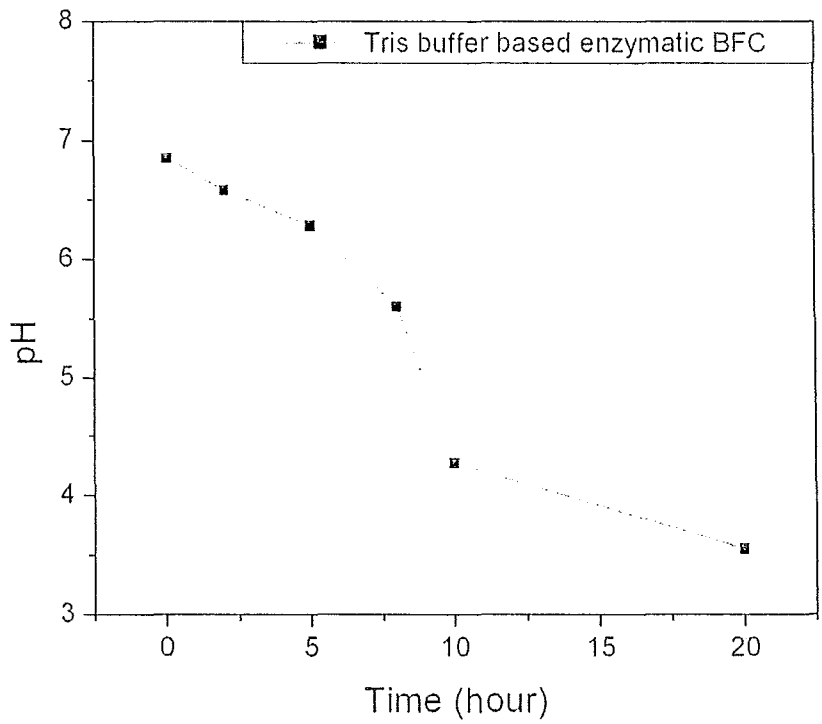

Figure 4.2 The pH value decreases vs. time in Tris buffer based enzymatic BFC.

4.4 Anion Exchange Membrane

Anion Exchange Membrane (AEM) is introduced to avoid the possible cation transport in Nafion. AEM is capable of conducting anions (e.g., OH^-), rather than cations in Nafion. Thus the anodic and cathodic reactions are modified according to the alkaline media, whereas the whole reaction stays the same.

Anode: $C_6H_{12}O_6$ (glucose) + $2OH^- \rightarrow C_6H_{10}O_6$ (gluconolactone) + $2H_2O + 2e^-$ (4.4)

Cathode: $1/2\ O_2 + H_2O + 2e^- \rightarrow 2\ OH^-$ (4.5)

Overall: $C_6H_{12}O_6$ (glucose) $+1/2\ O_2 \rightarrow C_6H_{10}O_6$ (gluconolactone) + H_2O (4.6)

Three different AEMs have been selected with various thickness and internal resistance. Fumasep FAB is based on crosslinked polypropylene substrate, AMI-7001s gel polystyrene crosslinked with divinylbenzene and Excellion Snowpure AEM polypropylene. Their thicknesses are 0.0812 mm, 0.4622 mm and 0.353 mm, respectively. The structures of AEMs are different but pertinently they all serve the same purpose.

The AEMs were mounted in our BFC, replacing Nafion in between the two electrode chambers. The polarization curves were measured step by step at 5 minute intervals. Meanwhile, the pH values were collected to find out whether the problem of pH gradient can be resolved.

4.4.1 Polarization Curves and Power Densities

When the polarization curves were tested, it was found that the currents were so small that few resistance loadings can be tried. And the maximum power density is much lower than Nafion based BFC. However, it is found that Fumasep FAB gives best performance (Figure 4.3 and 4.4), probably due to the smaller membrane resistance related to the thickness.

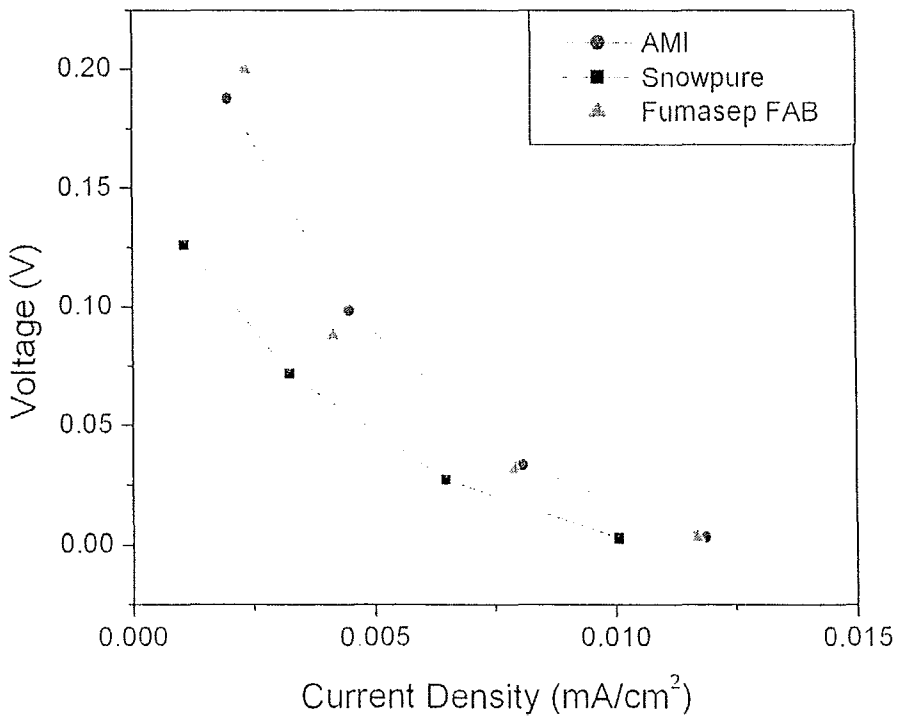

Figure 4.3 Polarization curves our enzymatic BFC with various AEMs.

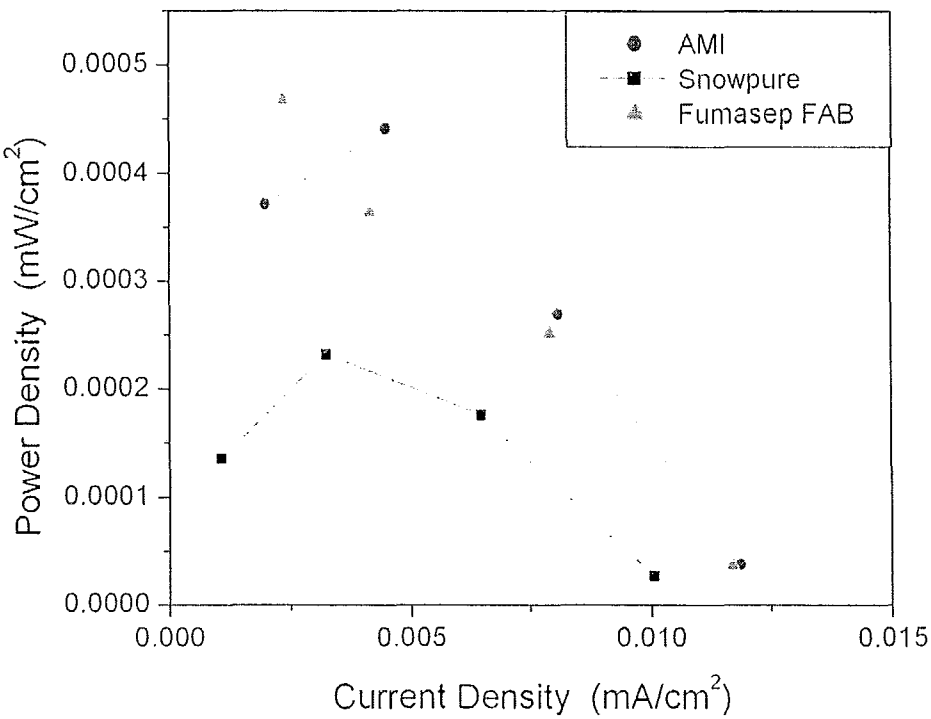

Figure 4.4 Power densities of our enzymatic BFC with various AEMs.

4.4.2 pH Result

The pH-time relationship is plotted in figure 4.5 where Fumasep FAB was used as the ion exchange membrane. Fumasep FAB is chosen for its best performance among all

the available alternatives as shown in Figure 4.3 and 4.4. Compared with Figure 4.1, the BFC system with AEM has little pH gradient problem and the pH stabilizes at the value of 6.30.

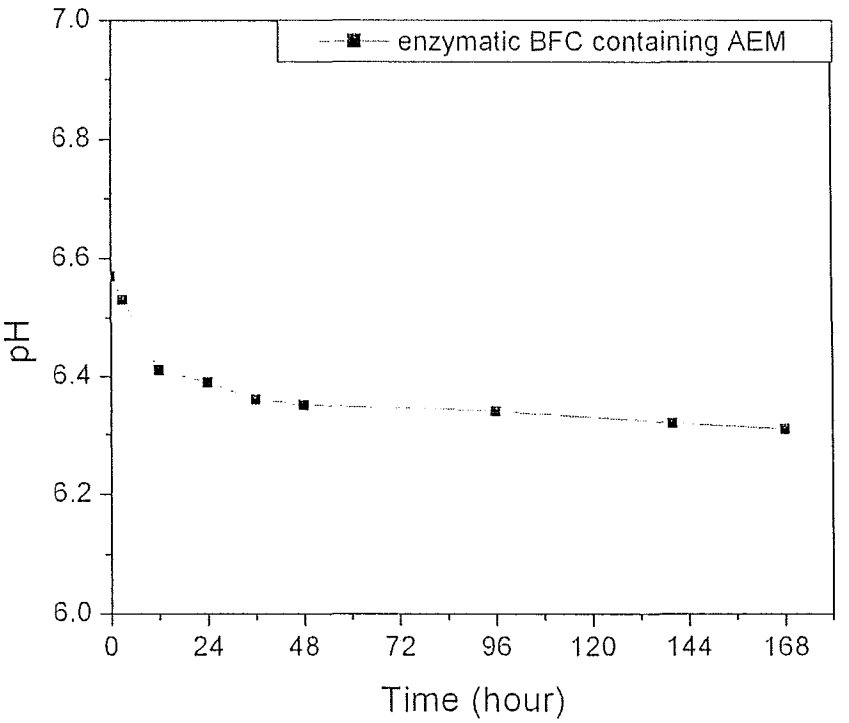

Figure 4.5 The pH value decreases vs. time in the AEM based enzymatic BFC.

To summarize, AEMs successfully suppressed the accumulation of protons at the anode, with only a little drop of pH value as shown in Figure 4.5. However, they could not increase the power density. The power output of AEM based BFC is even worse than

Nafion based BFC although the latter has severe pH gradient problem. Therefore, power density cannot be improved simply by changing the membrane inside the BFC and alternative configurations or mechanisms have to be searched in future.

Chapter 5 Uncovering an "Extra" Current

5.1 Paper Submitted

Extra current uncovered in alkaline biofuel cells

Cindy X. Zhao,† Kevin K. Wang,† Han Yan,† Quan Yang,‡ Doug K. Charles‡ and Gu Xu,†*

† Department of Materials Science & Engineering, McMaster University, Hamilton, Ontario, Canada L8S 4L7

‡ Vale Inco Ltd., 2060 Flavelle Boulevard, Sheridan Park, Mississauga, Ontario, Canada L5K 1Z9

* Corresponding author email address: xugu@mcmaster.ca.

Abstract

Due to the environmental burden of fossil fuel combustion, a major strategic shift towards renewable green sources and environmentally benign power generation technology makes biofuel cells a possible alternative, though their extremely low current density remains a bottleneck for the further practical applications. Recent progress shows some promise to increase the current by platinum (Pt) electrodes, and alkaline solution to replace the

enzymes/microbes. However, the approach involves high cost of noble metals as well as their poisoning effect. We report here a glucose biofuel cell based on nickel (Ni) electrodes and alkaline medium without the catalyst poisoning found in Pt systems. Surprisingly, a six-fold current increase over time, and a final current density equivalent to 1.5 times that of Pt have been achieved. They are found to be caused by the transformation of glucose to an enediol form, the expansion of triple phase boundaries where cathode reactions take place, and the enhancement of reaction kinetics by alkaline solution. The results not only provide a dramatic increase in current and overall biofuel cell performance, but also demonstrate a low cost approach to renewable source utilization, if corresponding designs can be implemented.

5.2 Poisoning Effect of Platinum Electrodes

We began our experiments by duplicating the results of Fujiwara et al with a similar setup using both neutral and alkaline media (2009). As depicted by Figure 5.1, retrograde polarization curves appeared under both media, which were found to be due to the poisoning of Pt electrodes. Experimentally, the current first increases then decreases, following the drop of the load resistance and the output voltage. This can be explained by the increasing poisoning rate at higher current densities overwhelming the anodic

oxidation rate (Sandia Report, 2005). Once the Pt surface starts to be poisoned, the effective number of catalyst sites will decrease, and the availability of catalytic sites will predominate the reaction rate at the anode, which determines the overall cell performance. Due to the irreversible Pt poisoning, this availability will decrease continuously, forcing the current to drop, even under the presence of a lower potential. The curves also suggest that the poisoning effect is more serious in neutral medium than in alkaline under the same conditions (Figure 5.1), which coincides with that of the literature (Wilde, Zhang, 1993).

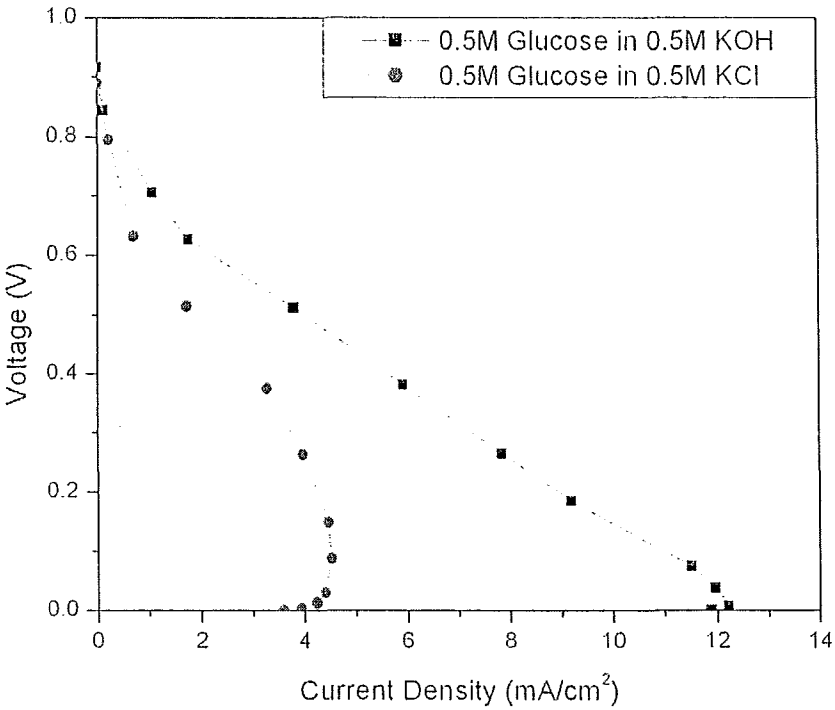

Figure 5.1 The polarization curves - the output voltage vs. current density of the BFC, using 0.5M glucose and 0.5M KCl anolyte (the circle dots), or 0.5M glucose and 0.5M KOH anolyte (the square dots). Anode: Pt-C black, cathode: Pt-C black, anion exchange membrane, cathode gas: humidified O_2 at 10 ml/min and room temperature.

5.3 Replacing Platinum by Nickel Catalyst

To remove the poisoning effect and high cost of Pt, Ni metal is proposed to take the place of Pt-C black and act as the electrocatalytic electrodes. The anodic, cathodic and overall reactions remain unchanged (Fujiwara et al., 2009):

Anode: $C_6H_{12}O_6$ (glucose) + 2 OH^- → $C_6H_{12}O_7$ (gluconic acid)+ H_2O +2e^- (5.1)

Cathode: 1/2 O_2 + H_2O +2e^- →2 OH^- (5.2)

Overall: $C_6H_{12}O_6$ (glucose) +1/2 O_2 → $C_6H_{12}O_7$ (gluconic acid) (5.3)

The new polarization curve is shown in Figure 5.2, where the poisoning effect is no longer observed, in contrast to the Pt case (Figure 5.1). The current density labeled under the horizontal axes is also noted as nominal current density, which is conventionally defined as the output current divided by the geometric or nominal area of the electrode surface. Although the geometric or nominal areas are similar for Ni and Pt (2.30 $cm^2$and 2.0 cm^2, respectively), the real or true surface areas are very different (Table 5.1). For the Ni electrode in our setup, which is only available in foam structure of 250 μm pore size and 90% porosity, the true surface area remains about 2.30 cm^2 (Table 5.2). However, an extremely larger number of 1200 cm^2 is found for the Pt electrode used

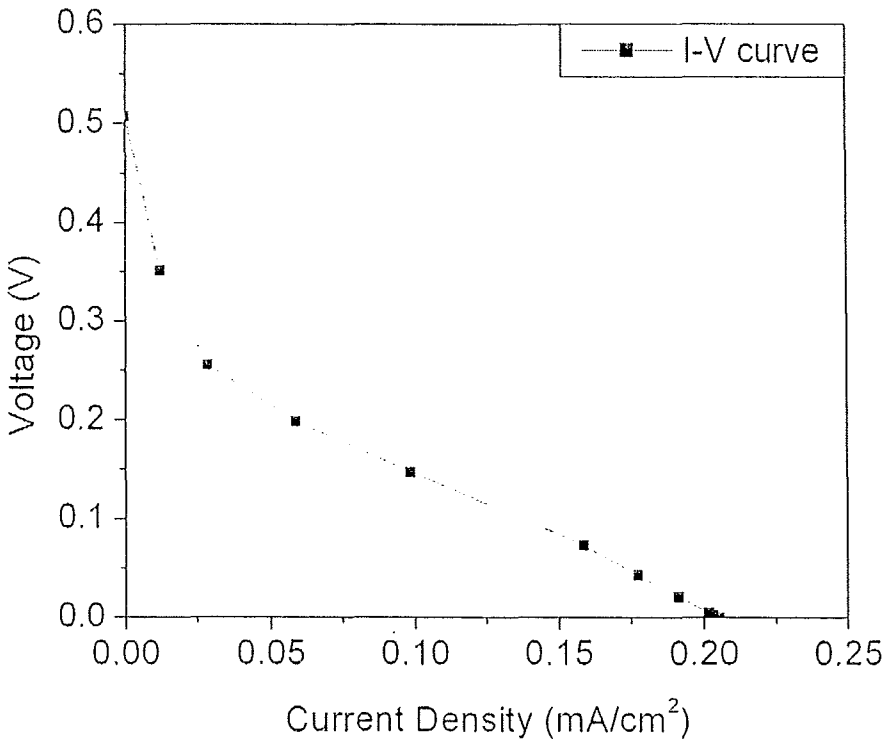

Figure 5.2 The new polarization curve of BFC based on Ni catalyst showing a maximum current density of 0.21mA/cm^2. Anode: Ni foam, cathode: Ni foam, anion exchange membrane, cathode gas: humidified O_2 at 10 ml/min and room temperature.

Table 5.1 Values of surface areas in nickel and platinum cases

Surface areas	Ours (cm^2)	Fujiwara et al. (cm^2)
Geometric (nominal) area	2.30	2
True surface (contour) area	2.30*	1200^+

*, based on the Ni foam of 250um pore size and 90% porosity

+, based on the Pt particles of 2.5 nanometer size, 3-D Pt-C structure.

Table 5.2 Values of current densities in nickel and platinum cases

Current densities	Initial results (mA/cm^2)	Fujiwara et al. (mA/cm^2)
Normalized by geometric (nominal) area	0.035	85
Normalized by true surface (contour) area	0.035	0.14

in Fujiwara's work, which is based on a catalyst loading of 3 mg/cm^2 and specific surface area of 20 m^2/g, involving 2.5 nm Pt particles and three dimensional membrane-electrode (PEMFC-MEA) structure (Fujiwara et al., 2009; Ren, Wilson, Gottesfeld, 1996). Therefore, a direct comparison of the nominal current densities with the Pt results is less meaningful, due to the perceptible differences between the structures and true surface areas of Ni and Pt. It should be more sensible to compare the true current densities, which are normalized by the true surface areas. Assuming the same true surface area can be achieved for Ni, initially, the maximum short-circuit current density normalized by the true surface area is found to be about a quarter of Fujiwara's result, viz., about 0.035 mA/cm^2 versus 0.14 mA/cm^2 (Fujiwara et al., 2009). In other words, although Ni foams involve no poisoning effect, they offer a current density 4 times lower than for Pt catalyst, based on an equivalent true surface area.

5.4 "Extra" Current Discovered

This result, however, tells only a partial story. A surprisingly high current density was obtained after 96 hours, if more than enough glucose was present. The total current rises by 6 times from 0.08 mA to 0.48 mA at 2.30 cm^2 as depicted in Figure 5.3, and result is repeatable. In addition, when normalized by the true surface area, the value of

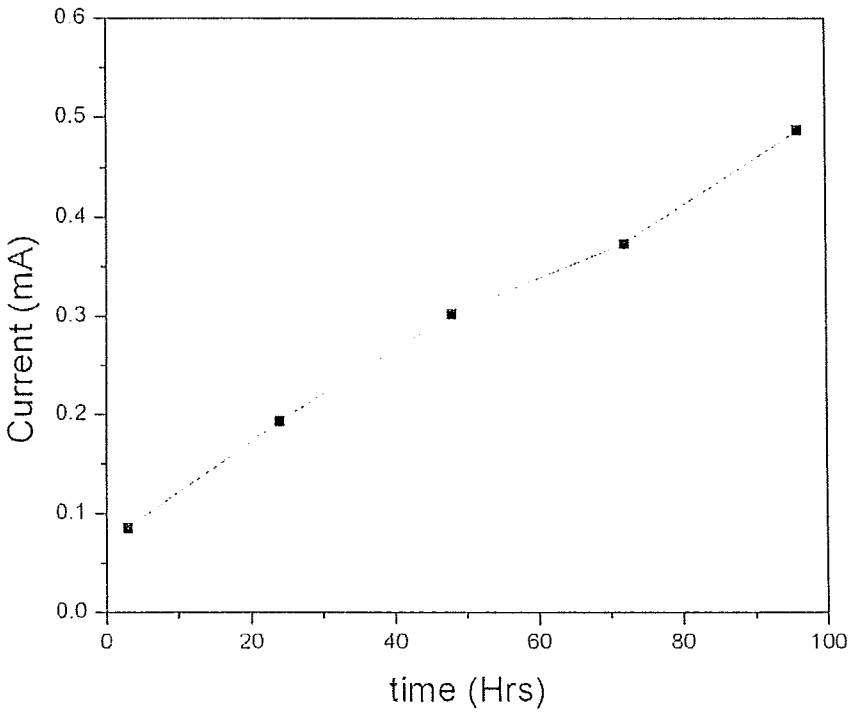

Figure 5.3 Six-fold current increase vs. time.

0.48 mA is equivalent to a true current density of 0.21 mA/cm^2, almost 1.5 times higher than that of Pt. This means, if Ni nano particles and a similar three dimensional structure (PEMFC-MEA) were employed, it would produce a nominal current density of 120 mA/cm^2.

The question now becomes, why such an extra increase of current is only

available after a long time operation. Fundamental analysis suggests that, first of all, it must correspond to the increase of flow rate of moving charges, viz., the electrons, which are produced by electrochemical reactions. Many factors could contribute to the increase, i.e., more reaction sites, "extra" electrochemistry or faster reaction kinetics, as shown in Scheme 5.1.

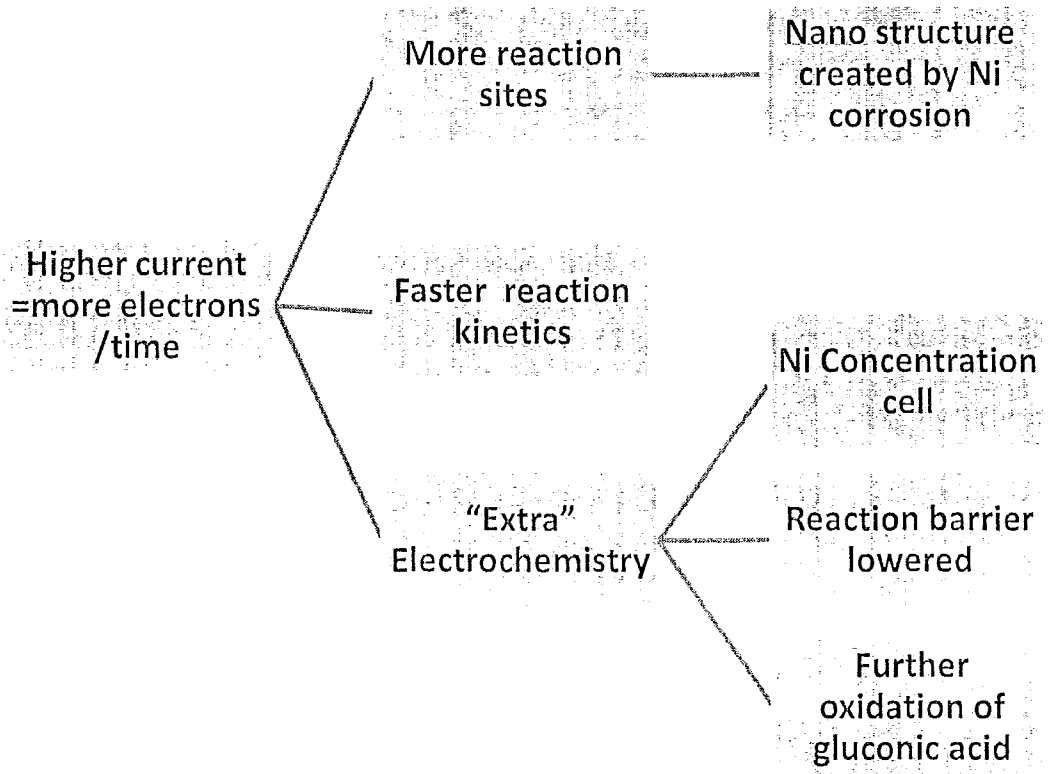

Scheme 5.1 Fundamental analysis of the six-fold current increase

5.4.1 Nickel Concentration Cell or Nickel Corrosion

A Ni concentration cell can be considered, in case Ni anode is corroded, which might also create nano structures by corrosion, to increase the surface area. If this was the case, the extra increase of current would be gained by Ni concentration cell itself or the subsequent Ni corrosion. However, this was rejected by experiments, due to the negligible weight loss of Ni anode.

Under the current of 0.48 mA for 24 hours, the Ni anode suffers almost no weight loss, which was smaller than 0.3 mg, compared with 12.6 mg, as predicted by the Faraday's law of electrolysis. The smaller weight loss than 0.3 mg is suggested to be due to the Ni redox couple needed for electron transfer and the equilibrium between deposited $Ni(OH)_2$ and dissolved Ni^{2+}, rather than the Ni corrosion at the anode (Luo, Zhang, Baldwin, 1991). That is, the extra current must not be related to the Ni electrode, a Ni concentration cell or surface area increase by possible nano structures created by Ni corrosion.

5.4.2 Further Oxidation of Gluconic Acid

Because of the complexity of oxidation of glucose and large number of

byproducts, the catalytic oxidation is then taken into consideration, which can be divided into two possibilities: one is the further oxidation of byproducts, the other is the transformation of glucose. The anodic reaction (5.1) shows a two-electron oxidation of glucose to gluconic acid. Although the further oxidation of gluconic acid might lose more than two electrons, it is impossible to increase the current density by 6 times. It is understood that gluconic acid formed on the Pt catalyst at pH=9 has the highest percentage of 87.5 as shown in Figure 5.4. It is also noted that the variation in pH of the media does not influence significantly the main product distribution (Abbadi, van Bekkum, 1995).

Consequently, a similar product distribution is expected in our case on Ni catalyst. Therefore, the probability is negligible for a glucose molecule to lose 4 or 6 electrons during the reaction.

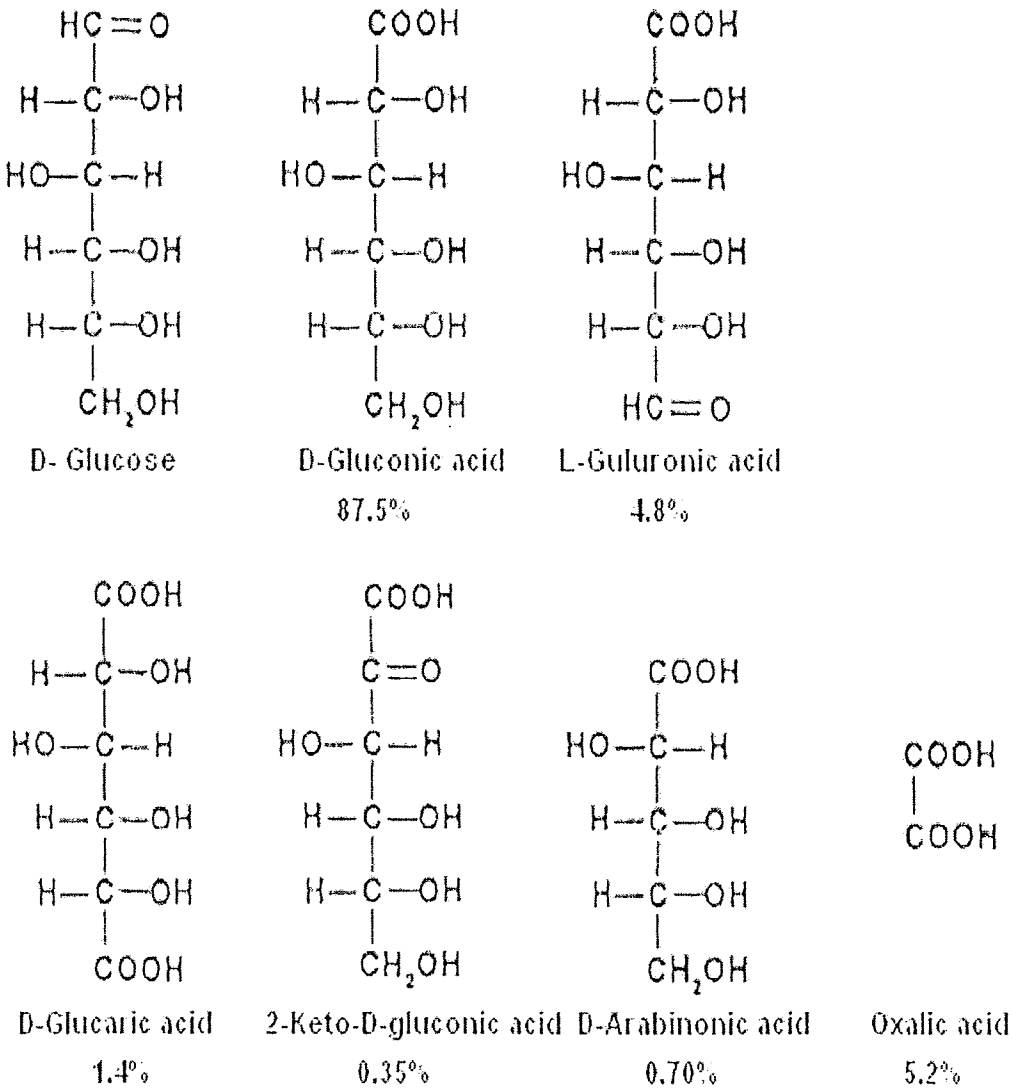

Figure 5.4 Glucose structure and main products (molar %) formed on Pt at pH=9 (Abbadi, van Bekkum, 1995)

5.4.3 Transformation of Glucose

It is possible, albeit complicated, to convert glucose to what is easier to be oxidized in alkaline solution to lower the reaction barrier. Experimentally it is found that the glucose solution prepared in alkaline medium gradually changes its color after 96 hours, from transparent to yellow-brownish (Figure 5.5).

According to Isbell et al (1969) and Nikolaeva et al (1983), glucose in alkaline solution could be transformed to become enediols involving double bonds of carbons (Figure 5.6), which give rise to a red wine-like color.

In our case, the color was indeed found to be associated with the presence of enediols. The extra increase of the current must be related to the color change, since gluconic acid and other products are all transparent, as supported by our ultraviolet-visible spectroscopy measurement. A strong absorption peak was found below 300 nm (Figure 5.7), which coincides with that of the literature, representing the peak of functional group of enediol around 250 nm (Jones, 1956; Ramirez, Tasaka, Desai, Smith, 1968).

It is well known that an object reflects light and absorbs the remaining spectra, leading to the fact that a color is determined by the wavelength of light reflection. For example, solution reflecting the red, green components of the spectrum leaves blue-violet absorbed. Thus, it verifies that the yellow-brownish color does come from the enediols.

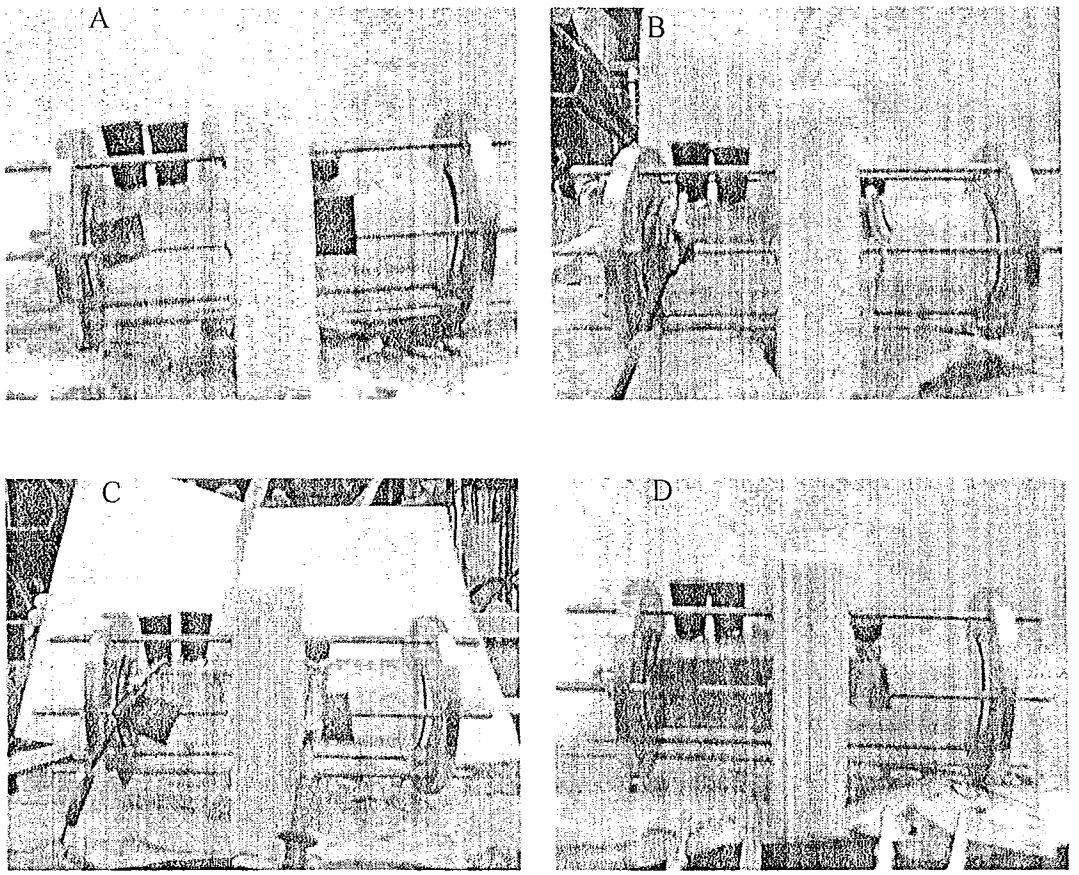

Figure 5.5 The anolyte color changes gradually over time, from transparent (A) to yellow-brownish (D) in 96 hours.

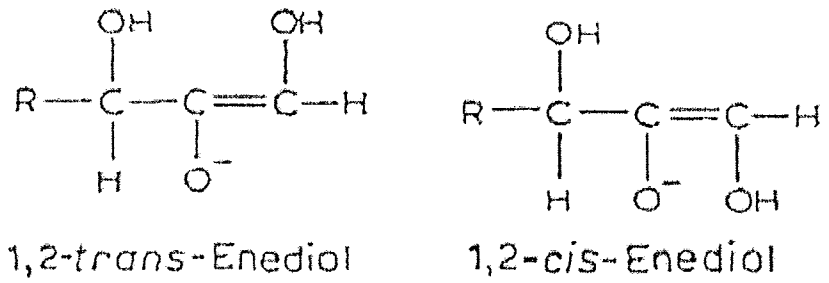

Figure 5.6 Possible forms of enediols found in glucose alkaline solution.

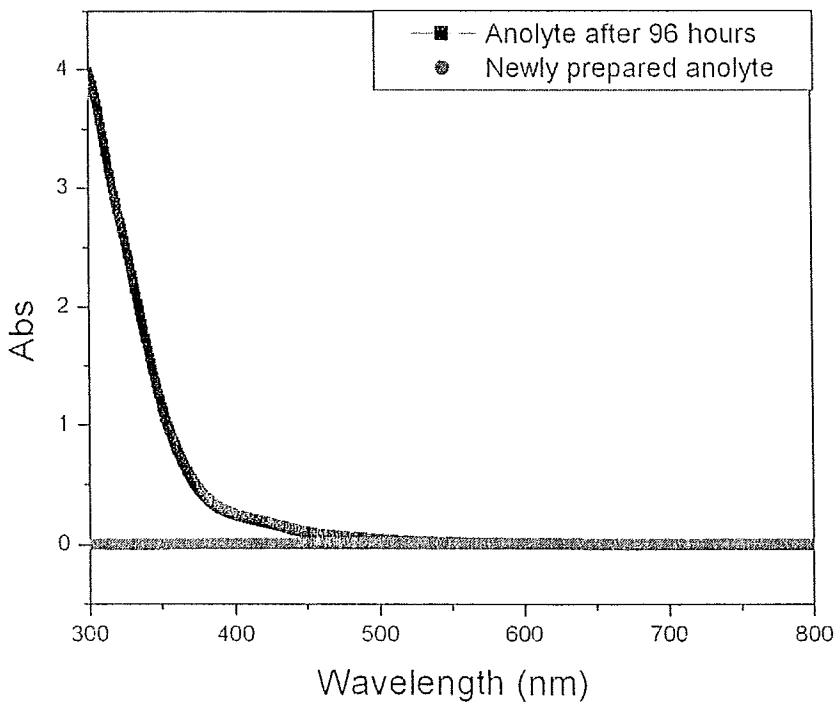

Figure 5.7 UV-Vis spectroscopy shows a strong absorption peak below 300 nm

The enediols may lower the oxidation reaction energy barrier, due to the recently proposed mechanism of, endiol anions from the principal enolization becoming the intermediate for the anodic reaction (Mor, Rubin, Schechner, 2008). Consequently, the current increase results from the enolization of glucose to the enediols.

To reconfirm the above findings, glucose in KOH solution was prepared separately and placed in empty vessels without the electrodes for 24, 48, 72 and 96 hours. A gradual color change from transparent to yellow-brownish was observed. Then the measurements were started with the prepared solutions. The current does increase over time as described in Figure 5.8. However, it only reaches 0.21 mA for the area of 2.3 cm^2, less than a half of the value before (0.48 mA).

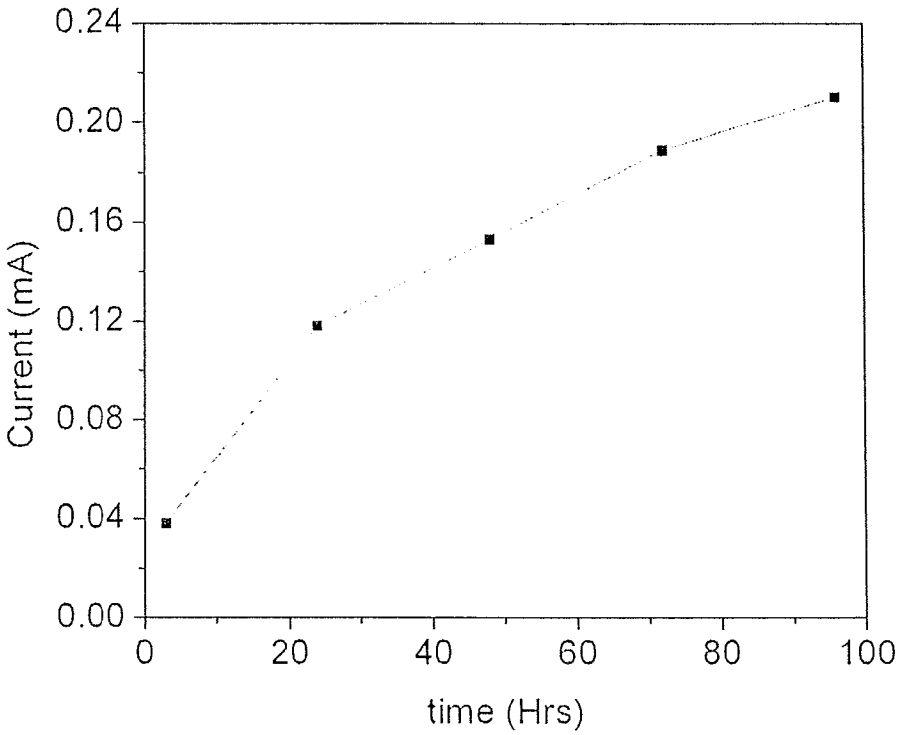

Figure 5.8 The current change vs. time involving glucose enolization effect.

5.5 "Extra" Current Increase Unravelled

All these seem to suggest that something else must be hidden, because the transformation of glucose to enediols cannot fully explain the extra current increase. To unravel the mystery, many trials were executed. Eventually, a small leak was found in the

setup, resulting in anolyte in contact with the cathode. Further analysis suggests the possibility of the increase of reaction sites and speed, as summarized in Scheme 5.2.

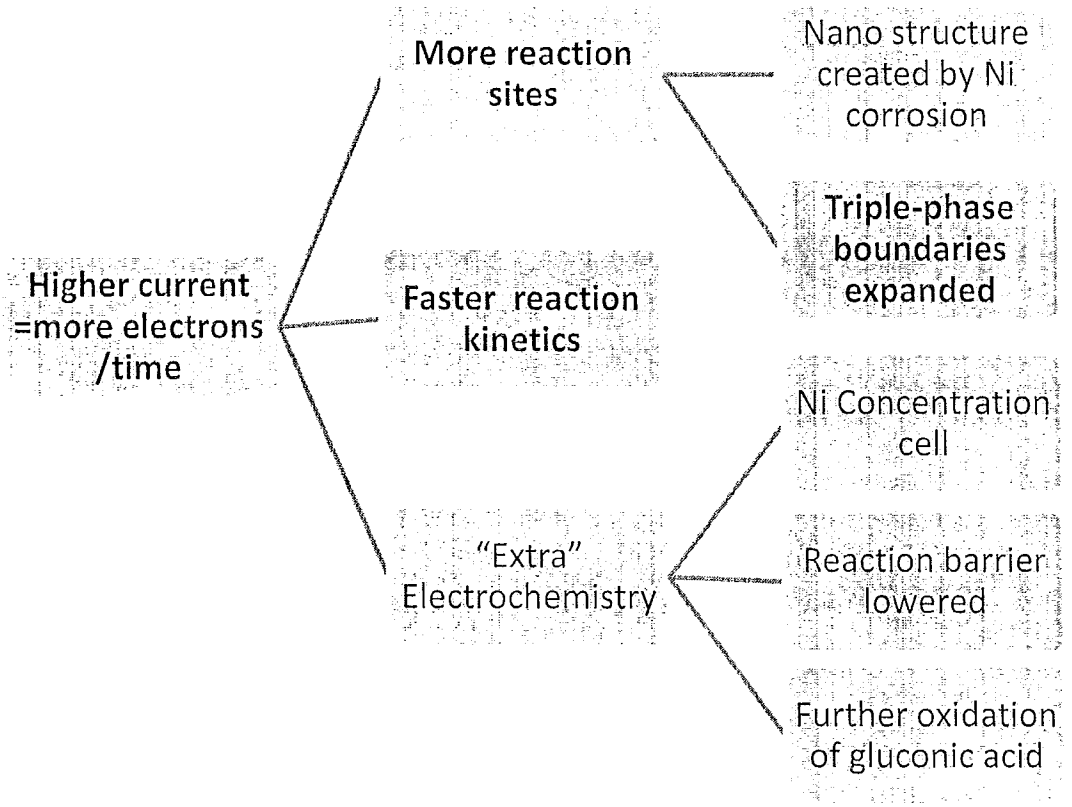

Scheme 5.2 Further analysis of the six-fold current increase

The situation was then simulated by various solutions purposely injected into the cathode. These experiments indeed produce additional current increase, as described in

Figure 5.9, where the up-triangular dots and square dots represent the situations with and without water injection at the cathode, respectively.

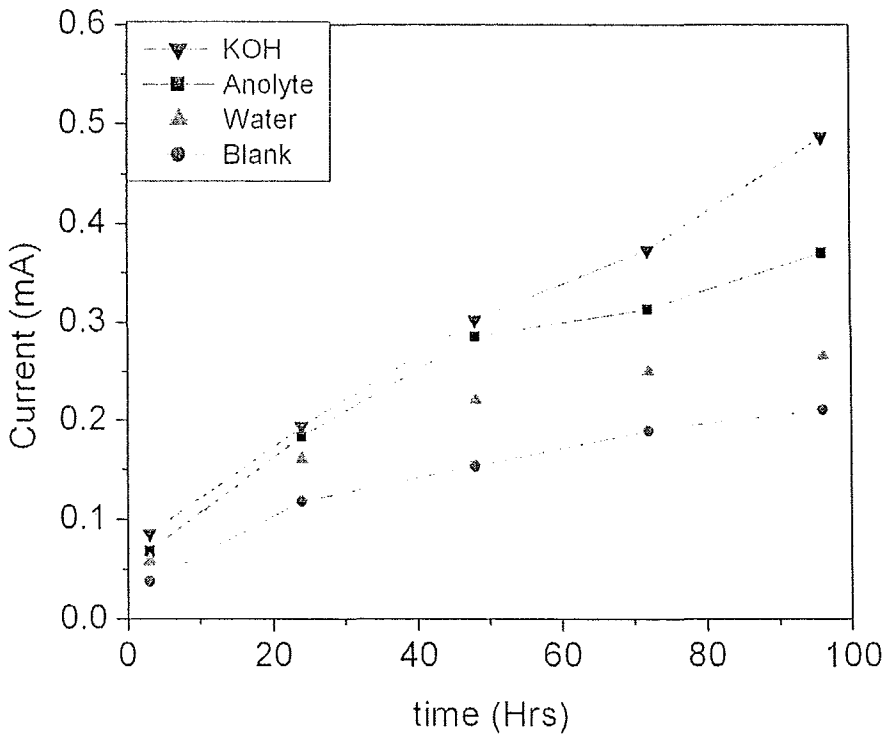

Figure 5.9 The current increases vs. time with various solutions purposely injected into the cathode.

5.5.1 Triple Phase Boundary Expansion

The increment, however, can be attributed to the triple phase boundary expansion. Since the electrochemical reaction is a surface related process, the cathodic reaction takes place at the triple phase boundaries. The solution injection basically expands the triple phase boundaries as depicted by Figure 5.10.

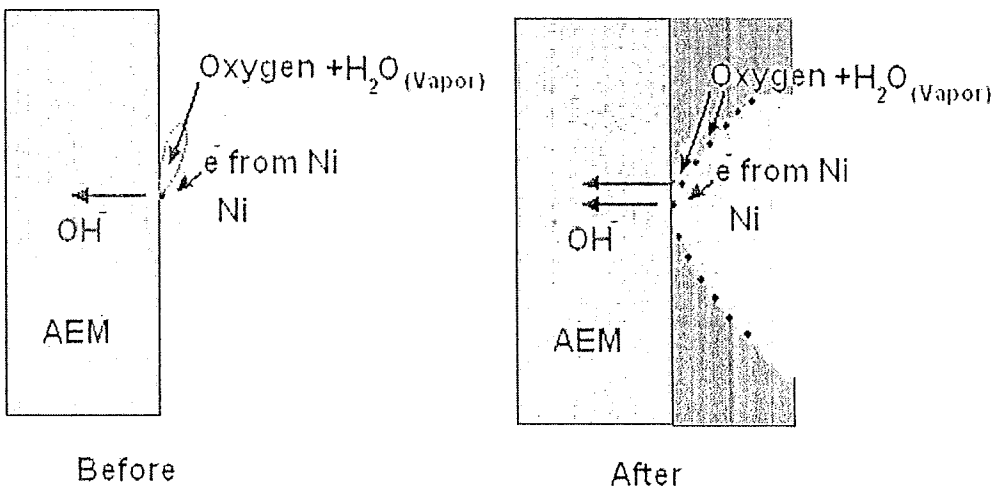

Figure 5.10 Schematic illustrating the expansion of triple phase boundaries by injection.

Before the injection, electrons are transported by Ni foam, humidified oxygen from the pore, and OH- migrate though the anion exchange membrane. All three phases meet at one point. If the solution is injected into the cathode and fills the pores as

indicated by the colored area, the oxygen has to be dissolved in the solution first and OH- has to migrate through the solution, then the anion exchange membrane. As a result, the triple phase boundaries expand from one point to a finite area and provide more reaction sites at the cathode and hence current increases.

5.5.2 Faster Reaction Kinetics

It is also found that the cell with KOH injection has the best performance among others, followed by the KOH containing anolyte and water. The increments from the up-triangular dots to square dots, or from the up-triangular dots to down-triangular dots, are not only related to the triple phase boundary expansion, but also attributed to either the conductivity increase, or the cathode kinetics enhancement.

Water injection, represented by the up-triangular dots, will increase the reactant concentration, according to the cathodic reaction (5.2). Low water concentration, caused by the lack of humidity in the bubbling gas supplier, limits the cathodic reaction. If enough water is provided, the cathodic reaction can be promoted and consequently the current increases. In addition, the KOH solution and anolyte having better ion conductivity could reduce the internal resistance against the OH- migration. That is, the current increases due to the reduction of internal ohmic loss. Furthermore, the presence of

KOH at the cathode enhances oxygen reduction by enhanced kinetics and a lower degree of specific anion adsorption (Spendelow, Wieckowshi, 2007). The reaction kinetics of the cathodic reduction of oxygen in alkaline medium is therefore higher than in acidic or neutral medium (Fujiwara et al., 2009).

Chapter 6 Conclusions

Due to the environmental burden of fossil fuel combustion, a major strategic shift towards renewable green sources and environmentally benign power generation technology makes biofuel cells a possible alternative, though their extremely low current density remains a bottleneck for the further practical applications. Recent progress shows some promise to increase the current by Pt electrodes, and alkaline solution to replace the enzymes/microbes. However, the approach involves high cost of noble metals as well as their poisoning effect.

In this thesis, the poisoning effect of Pt electrodes in a glucose BFC is first confirmed, resulting in the need of other catalytic metals. Ni metal is then introduced, and a glucose BFC based on Ni foams and alkaline medium shows no catalyst poisoning effect as found in the Pt system. In addition, a six-fold current increase over time, and a final current density equivalent to 1.5 times that of Pt have been achieved. They are found to be caused by the transformation of glucose to enediol forms which involve carbon double bonds, the expansion of triple phase boundaries where cathode reactions take place, and the enhancement of reaction kinetics by alkaline solution.

The possibility of the same current increase in the case of Pt-C black, however,

may be obscured by the fact that a long enough time is needed. Through possible new designs, such as wet cathode and treated glucose, the results not only provide a dramatic increase in current output thus the overall biofuel cell performance, but also demonstrate a low cost approach to renewable source utilization.

Chapter 7 Future Work

Already discovered are the positive effects of the transformation of glucose to an enediol form which can lower the reaction barrier, the expansion of triple phase boundaries where cathode reactions take place, and the enhanced reaction kinetics by alkaline solution injection. Also, it is found that using a multiple layer of Ni foams at the anode could further increase the current due to the enlarged effective surface area. However, the current does not increase linearly with the number of Ni foams lying at the anode, hence there must be some rate-limiting factors hindering the current growth. Therefore, it is proposed that the exploration of Ni catalyst will continue and nano Ni particles will be searched to be used in Ni-MEA structure as suggested by the previous chapters.

Based on what has been accomplished in the biofuel cell area, future research into organic solar cells is also proposed, where both are falling into the category of energy conversion devices, except the former rely on ionic conduction of the electrolyte separating anode and cathode, whereas the latter involve p-n junctions to split electrons and holes.

The similarities between fuel cells and solar cells allow for the extension of the

findings made in this thesis, to the possible improvement of the state-of-art established to organic solar cells today. For example, the triple phase boundaries are expanded by the liquid in contact with the solid interfaces.

As is well known, the organic solar cells suffer from the low energy efficiency (< 6.5%), in spite of their huge potentials of low cost fabrication to over take the main stream of silicon solar cells today (Gerl, 2005). Tandem structures and fluorescent dyes offer a tremendous opportunity, but in the meantime pose big challenges to the in-depth level of device physics and design, which nevertheless bear relationships to electrochemical devices such as fuel cells, especially when involve lifetime issues (Kim et al., 2007; Nattestard et al., 2010).

A typical organic tandem cell comprised of two distinct devices stacked on top of each other, each of them being based on a Donor–Acceptor composite. The light which is not absorbed in the bottom device can further impinge on the top cell. Moreover, the thermalisation losses, viz., the wasted portion of photon energy beyond the "band gap" are lowered due to the usage of materials having different band gaps. The two cells involved in the device can be connected either in series (two-terminal) or in parallel (three-terminal), depending on the nature of the intermediate layer and on the way the intermediate layer and the two electrodes are connected. The intermediate layer should ensure the alignment of the quasi-Fermi level of the acceptor of the bottom cell with the

quasi-Fermi level of the donor of the top cell. In other words, the intermediate layer should allow the recombination of holes coming from one sub-cell with electrons coming from the other. Although it imposes great restrictions on the material selection and device design, an infinite number of devices can be piled up following the same principle.

So far, in the field of organic solar cells, a vast variation in designs involving a tandem structure has been considered, from small molecule evaporated materials up to fully solution-processed approaches, with various types of intermediate layers. The most efficient tandem organic solar cell reported by Heeger's group has around 6.5% power conversion efficiency (Kim et al., 2007). On the other hand, maximum efficiencies of 15% are expected for an optimized material couple.

The recent trend of utilizing the tandem structures and design rules suggest the opportunity for further improvement by more efficient materials, more functional intermediate layers and better matching of the materials with complimentary absorption spectra.

References

Abbadi, A., & van Bekkum, H. (1995). Effect of pH in the Pt-catalyzed oxidation of D-glucose to D-gluconic acid. *J. Mol. Catal. A-Chem.*, *97*, 111.

Anita. (2010, January 14). Eco Friendly Mobile Phone By Daizi Zheng For Nokia. Retrieved from http://www.envirogadget.com/alternative-energy/eco-friendly-mobile-phone-by-daizi-zheng-for-nokia/

Barton, S. C., Gallaway, J., & Atanassov, P. (2004). Enzymatic biofuel cells for implantable and microscale devices. *Chem. Rev.*, *104*, 4867.

Bullen, R. A., Arnot, T. C., Lakeman, J. B., & Walsh, F. C. (2006). Biofuel cells and their development. *Biosens. Bioelectron.*, *21*, 2015.

Chae, K. J., Choi, M., Ajayi, F. F., Park, W. S., Chang, I. S., & Kim, I. S. (2008). Mass Transport though a Proton Exchange Membrane (Nafion) in Microbial Fuel Cells. *Energ. Fuel.*, *22*, 169.

Fleischmann, M., Korinek, K., & Pletcher, D. (1971). The oxidation of organic compounds at a nickel anode in alkaline solution. *J. Electroanal. Chem.*, *31*, 39.

Fleischmann, M., Korinek, K., & Pletcher, D. (1972) The kinetics and mechanism of the oxidation of amines and alcohols at oxide-covered nickel, silver, copper, and cobalt electrodes. *J. Chem. Soc. Perkin. Trans. II*, *10*, 1396.

Fujiwara, N., Yamazaki, S., Siroma, Z., Ioroi, T., Senoh, H., & Yasuda, K. (2009). Nonenzymatic glucose fuel cells with an anion exchange membrane as an electrolyte. *Electrochem. Commun.*, *11*, 390.

Gerl, B. (2005). Photons from flexible plastics. *Pictures of the Future*, *Spring*, 64.

Haselkorn, A. (2002, August 28). Microbial Fuel Cells to Power Future. *The Daily Californian*, Berkeley, California.
Retrieved from http://www.me.berkeley.edu/~lwlin/news/Microbial.pdf

Isbell, H. S., Frush, H. L., Wade, C. W. R., & Hunter, C. E. (1969). Transformations of sugars in alkaline solutions. *Carbohyd. Res.*, *9*, 163.

Jones, R. N. (1945). The ultraviolet absorption Spectrum of 9,9'-phenanthroin. *J. Am. Chem. Soc.*, *67*, 1956.

Kartha, S., & Grimes, P. (1994). Fuel cells: energy conversion for the next century. *Phys. Today*, *47*, 54.

Katz, E., & Willner, I. (2003). A biofuel cell with electrochemically switchable and tunable power output. *J. Am. Chem. Soc., 125*, 6803.

Kim, J. R., Cheng, S. A., Oh, S. E., & Logan, B. E. (2007). Power generation using different cation, anion, and ultrafiltration membranes in Microbial Fuel Cells. *Environ. Sci. Technol.*, *41*, 1004.

Kim, J. Y., Lee, K., Coates, N. E., Moses, D., Nguyen, T. Q., Dante, M., & Heeger, A. J. (2007). Efficient tandem polymer solar cells fabricated by all-solution processing. *Science*, *317*, 222.

Liu, H., & Logan, B. E. (2004). Electricity generation using an air-cathode single chamber microbial fuel cell in the presence and absence of a proton exchange membrane. *Environ. Sci. Technol.*, *38*, 4044.

Logan, B. E., Hamelers, B., Rozendal, R. A., Schroder, U., Keller, J., Freguia, S., Aelterman, P., Verstraete, W., & Rabaey, K. (2006). Microbial fuel cells: methodology and technology. *Environ. Sci. Technol.*, *40,* 5181.

Luo, P., Zhang, F., & Baldwin, R. P. (1991). Comparison of metallic electrodes for constant-potential amperometric detection of carbohydrates, amino acids and related compounds in flow systems. *Anal. Chim. Acta.*, *244*, 169.

Mor, L., Rubin, Z., & Schechner, P. (2008). Measuring open circuit voltage in a glucose

alkaline fuel cell operationed as a continuous stirred tank reactor. *J. Fuel Cell Sci. Tech.*, *5*, 014503.

Nattestad, A., Mozer, A. J., Fischer, M. K. R., Cheng, Y. B., Mishra, A., Bäuerle, P., & Bach, U. (2010). Highly efficient photocathodes for dye-sensitized tandem solar cells. *Nat. Mater.*, *9*, 31.

Nikolaeva, N. N., Khazova, O. A., Vasilyev, & Yu. B. (1983). Kinetics and mechanism of the oxidation of flucose on a platinum electrode. *Elektrokhimiya*, *19*, 1476.

Ramirez, F., Tasaka, K., Desai, N. B., & Smith, C. P. (1968). α-bromo-α-ketol phosphates and enediol bisphosphates. *J. Org. Chem.*, *33*, 25.

Ren, X., Wilson, M. S., & Gottesfeld, S. (1996). High performance direct methanol polymer electrolyte fuel cells. *J. Electrochem. Soc.*, *143*, L12.

Rozendal, R. A., Hamelers, H. V. M., & Buisman, C. J. N. (2006). Effects of membrane cation transport on pH and microbial fuel cell performance. *Environ. Sci. Technol.*, *40*, 5206.

Rozendal, R. A., Hamelers, H. V. M., Molenkamp, R. J., & Buisman, C. J. N. (2007). Performance of single chamber biocatalyzed electrolysis with different types of ion exchange membranes. *Water Res.*, *41*, 1984.

Rozendal, R. A., Hamelers, H. V. M., Rabaey, K., Keller, J., & Buisman, C. J. N. (2008). Towards practical implementation of bioelectrochemical wastewater treatment. *Trends Biotechnol.*, *26*, 450.

Sakai, H., Nakagawa, T., Tokita, Y., Hatazawa, T., Ikeda, T., Tsujimura, S., & Kano, K. (2009). A high-power glucose/oxygen biofuel cell operating under quiescent conditions. *Energy Environ. Sci.*, *2*, 133.

Sandia Report SAND2005-5734. (2005). *Bio micro fuel cell grand challenge final report*, Sandia National Laboratories: Albuquerque, NM, 2005.
Retrieved from http://www.osti.gov/bridge/product.biblio.jsp?osti_id=876287.

Shukla, A.K., Suresh, P., Berchmans, S. & Rajendran, A. (2004). Biological fuel cells and

their applications. *Current Science, 87*, 455.

SONY (2007, August 23). Sony Develops "Bio Battery" Generating Electricity from Sugar. Retrieved from http://www.sony.net/SonyInfo/News/Press/200708/07-074E/index.html

Soukharev, V., Mano, N., & Heller, A. (2004). A four-electron O_2-electroreduction biocatalyst superior to platinum and a biofuel cell operating at 0.88 V. *J. Am. Chem. Soc., 126*, 8368.

Spendelow, J. S., & Wieckowshi, A. (2007). Electrocatalysis of oxygen reduction and small alcohol oxidation in alkaline media. *Phys. Chem. Chem. Phys., 9*, 2654.

Tsujimura, S., Kano, K., & Ikeda, T. (2002). Glucose/O_2 biofuel cell operating at physiological conditions. *Electrochemistry, 70*, 940.

Wilde, C. P., & Zhang, M. (1993). Oxidation of glucose at electrodeposited platinum electrodes in alkaline solution. *J. Chem. Soc. Faraday Trans., 89*, 385.

Wilkinson, S. (2000). Gastrobots – benefits and challenges of microbial fuel cells in food powered robot applications. *Autonomous Robots, 9*, 99.

Zhao, C., Shao, C., Li, M., & Jiao, K. (2007). Flow-injection analysis of glucose without enzyme based on electrocatalytic oxidation of glucose at a nickel electrode. *Talanta, 71*, 1769.

Zhao, C. X, Wang, K. K., Yan, H., Yang, Q., Charles, D. K., & Xu, G. (2010). Extra current uncovered in alkaline biofuel cells. *Submitted.*

Zhi, M. (2006). The rate-limiting step in a glucose/oxygen biofuel cell. M. A. Sc. Dissertation, McMaster University, Hamilton, ON.